IHE DELFT Institute for Water Education
under the auspices of UNESCO

Flood Impact Estimates for Europe due to Extreme Sea Levels

Investigation on expanding the use of reduced-physics solver SFINCS

Hassaan Mohamed

MSc Thesis Identifier - WSE-CEPD.23-05
April 2023

Flood Impact Estimates for Europe due to Extreme Sea Levels

Master of Science Thesis
by
Hassaan Mohamed

Supervisors
Prof. Roshanka Ranasinghe (IHE Delft)

Mentors
Johan Reyns (IHE Delft)

Examination Committee
Prof. Roshanka Ranasinghe
Johan Reyns
Dr. Timothy Tiggeloven

This research is done for the partial fulfilment of requirements for the Master of Science degree at the IHE Delft Institute for Water Education, Delft, the Netherlands.

Delft
04/04/2023

Image Credit: Flicker
(https://www.flickr.com/photos/16633132@N04/16265764022/in/photostream/)
(Photograph taken by Ronnie Robertson)

Date Taken: 12 January 2015

Location Taken: Scottish coast

“We are heading into a disaster...we have waged war on nature, and nature is striking back, and striking back in a devastating way.”

UN Secretary-General Antonio Guterres regarding the floods in Pakistan

“We are, after all, the greatest problem solvers to have ever existed on Earth. If working apart, we are a force powerful enough to destabilize our planet. Surely working together, we are powerful enough to save it.”

Naturalist Sir David Attenborough at COP26

Abstract

Coastal zones are highly populated and developed land areas throughout the world and this trend is expected to continue in the future given their popularity in terms of recreational, economic, and ecological factors. However, these coastal zones are highly vulnerable locations to a range of socio-economic and environmental threats such as impacts due to extreme sea levels and climate change. Extreme sea levels are a result of compound effects from tides, waves, and storm surges. With the threat of sea level rise and climate change driven variations in extreme meteorological events such as increased storm wave heights plus surge frequencies, extreme water levels would result in a higher rate of episodic inundation and coastal flooding events in the future. Hence assessment of these flooding scenarios is critical to evaluate the risk these zones face and develop adaption and mitigation strategies.

The overarching objective of this study is to develop and assess a methodology for applying the reduced-physics solver SFINCS on a large-scale to estimate flood impacts caused by extreme sea levels. This was achieved by generating the required input files for the SFINCS models via MATLAB and QGIS. A detailed outline of how the scaling-up process was conducted is provided. This procedure includes a semi-automated process for the generation of grids along the coastline, assigning elevation and spatially varying friction data to the grid cells, producing and applying synthetic hydrographs as boundary conditions, and implementing flood protection levels along the coastline from available data. The methodology and subsequent models were then tested for different locations along the European coast.

The outputs from the SFINCS models were compared against flood estimates from a GIS based inundation model. Flooded areas and flood extent were assessed by utilizing fit metrics hit ratios, critical success index, and false alarm ratios. Maximum water levels obtained from the simulations were used for the comparative analysis of the models. The results indicated that while the model estimates align in certain locations, discrepancies are present in other test locations. A significant trend in results for both flood depths and fit metrics was not seen from the results evaluated. This is most likely due to differences in their modelling techniques and the inherent uncertainties involved in each approach. Limitations in model resolution, flood protection levels, boundary conditions, and friction values were highlighted.

In conclusion, the results from the SFINCS were deemed acceptable and within an expected range free of unrealistic outputs. The methodology was successfully implemented and the performance of the solver at this scale could also be considered computationally efficient, subject to the utilization of the recommended high-performance computers. This gives the potential to further assess the validity of the SFINCS solver and study various applicable scenarios related to coastal flooding in the future.

Acknowledgements

I am grateful to IHE Delft and the Dutch Ministry of Foreign Affairs for the opportunity to undertake my postgraduate studies here in Delft, Netherlands via the SIDS scholarship. Being from Maldives, I have always wanted to expand my knowledge in engineering within the water sector. It was a dream come true to study coastal engineering in Netherlands, a well-recognized worldwide leader in this sector with a history of effective coastal management, protection and innovation. Time at IHE Delft was challenging but it has been a truly remarkable experience and I have cherished every moment of it.

I would like to thank Johan and Rosh for expressing their interest to carry out this study with me. They have been very supportive throughout the process and always encouraged me to do better. Special thanks and appreciation to Johan for being patient with me, answering my various queries and for the guidance provided whenever needed, without which I would not have gotten this far. Also, my sincere gratitude to all the Coastal department lecturers, Alvaro, Dano, Ali, Mick, Ap and the external lecturers who shared their invaluable knowledge and experiences though out the Masters' program.

Deepest gratitude to my partner, Shuau for being there for me and supporting me from afar. Her words of encouragement and belief in me has been instrumental in getting through this process and I am truly grateful to have her by my side. In the same breath, I would also like to acknowledge my parents for their unwavering support and the sacrifices they have made for me to reach my goals. Furthermore, special thanks to my sister and friend Raidha, for always being helpful, a positive influence and a source of joy. I am looking forward to seeing them again soon.

Lastly, I want to acknowledge my friends who have also been on this IHE journey with me. These include my fellow Maldivians, whose help and engaging conversations have lifted me up in various ways during my time here. I also feel very fortunate to connect with people from diverse backgrounds and got the chance to learn a lot from them. Special mention to everyone from the "Straat Vybz" and "Summerhouse" groups for making my time here in Netherlands an incredible experience. The lunch times, football & basketball games, our trips together, study sessions and just hanging out in general, made my Masters journey really enjoyable and I will miss them greatly.

Table of Contents

List of Figures

List of Tables

Abbreviations

Acronyms	Description
AM	Annual Maxima
CC	Climate Change
COP-DEM	Copernicus Digital Elevation Model
DEM	Digital Elevation Model
DRC	Dynamic Reduced-Complexity
ESL	Extreme Sea Level
EVA	Extreme Value Analysis
FA	Flooded Area
GCM	Global Climate Model
GIS	Graphical Information System
GWSE	Global Surface Water Explorer
IPCC	Intergovernmental Panel on Climate Change
LAC	LISFLOOD -AC
LECZ	Low Elevation Coastal Zones
LFP	LISFLOOD-FP
LIE	Local Inertia Equations
MATLAB	Matrix Laboratory
MSL	Mean Sea Level
NHSWE	Non-hydrostatic shallow water equations
PDF	Probability Distribution Function
RCP	Representative Concentration Pathway
RSLC	Relative Sea Level Change
RSLR	Relative Sea Level Rise
SFINCS	Super-Fast Inundation of CoastS
SLR	Sea level rise
SPM	Shore Protection Manual
SRTM	Shuttle Radar Topography
SSWE	Simplified Shallow Water Equations
SWASH	Simulating Waves till Shore
SWE	Shallow Water Equations
TSL	Total Sea Level
XBeach	Extreme Beach behaviour model
Xbeach-nh	Xbeach Non-hydrostatic model

List of Symbols

Roman Letters	Description	Unit
F_m	Flooded area estimated by the model	m^2 or km^2
F_o	Observed flooded area	m^2 or km^2
g	Gravitational acceleration	m^2/s
h_{max}	Maximum water depth	m
t	time	s
x	Location in the horizontal direction	m
y	Location in the vertical direction	m
Zs_{max}	Maximum water level output from SFINCS	cm

Greek Letters	Description	Unit
η	Water levels	m
$\boldsymbol{\alpha}$	Heuristic time step reduction factor	-

Chapter 1 Introduction

This chapter presents the relevant background information and introduces this thesis research. Additionally, the problem statement, motivation for the research, objectives plus questions to be resolved during the research and its significance is provided.

1.1 Background

Coastal zones are the most populated and developed land areas in the world with population densities exceeding three times that of the global average (Small and Nicholls, 2003). This is a clear indication of their significance for decision makers, scientific community and the general public. Coasts provide attractive locations for urbanisation and tourism, resulting in fast economic and population growth (Nicholls, et al., 2007). Small and Nicholls (2003) estimates that around 23% of the global population reside less than 100 km from the shore plus no more than 100 m above sea level and roughly 10% of the overall population lives at elevations below 10 m above mean sea level, that is defined as low elevation coastal zones (LECZ) consisting of small island countries and populous deltaic regions (McGranahan, et al., 2016). Given the popularity of these coastal zones, these numbers are expected to increase significantly in the future (Curtis and Schneider, 2011).

Although settlements and economic activity is high and growing significantly in these coastal zones, they are recognized as exceedingly vulnerable locations. Coastal communities and ecosystems are susceptible to major socio-economic and environmental impacts due extreme sea levels (ESLs) (Hallegatte, et al., 2013, Hinkel, et al., 2014) and climate change (CC) (Hinkel, et al., 2013, Ranasinghe, 2016, Vousdoukas, et al., 2018a). According to Gregory, et al. (2019) ESL is defined as “an extraordinarily high or low local sea-surface level”. This is potentially the result of a compound effect of tides, waves and storm surges (Tebaldi, et al., 2021). It is also important to highlight that relative sea-level change (RSLC) is deemed to have a bigger impact in projected ESLs than variations in future atmospheric forcing (Gregory, et al., 2019). Coastal flooding is caused by a combination of the various coastal drivers including CC driven sea level changes and neglecting their compounding effect can lead to underestimation of the flood severity (Marcos, et al., 2019). Hence, ESLs can be considered a critical component in coastal flooding and therefore understanding it’s evolution into the future is also essential for comprehensive flooding assessments.

Sea level rise (SLR) is serious threat to the coastal communities (Hinkel, et al., 2014) and the CC driven variations in extreme meteorological events can exacerbate the impact of this rise (Vousdoukas, et al., 2016). Nicholls, et al. (1999), states that considering the projected SLR, the annual average of people experiencing flooding could increase by more than 5 times. This raises further concerns given that recent studies have indicated that SLR is increasing at an accelerated rate within the past 3 decades (Dangendorf, et al., 2019) and is expected to increase

substantially throughout the 21st century (Nicholls, et al., 2021). Coastal zones can reduce the impact of these issues by utilizing efficient hazard assessments via flooding/inundation maps that can be critical in a broad range of coastal management and engineering practices (Vousdoukas, et al., 2016).

The literature refers to three general methodologies in simulating coastal flooding. Simple static inundation, reduced complexity or physics models and full-physics process-based models (Leijnse, et al., 2021). SFINCS (Super-Fast INundation of CoastS) solver is one of the possible intermediate reduced-physics approaches that could be researched to evaluate coastal flooding extents on a continental scale and contribute to the limited information in mapping coastal flood hazards.

1.2 Motivation and Significance

The compounding effects of SLR, higher magnitudes of storm wave height and storm surge frequencies would result in more cases of episodic inundation or flooding events in the future (Ranasinghe, 2016). This is a challenge for coastal and flood risk management and pose serious consequences to vulnerable coastal regions if not acted upon appropriately. CC together with subsidence of land can potentially result in extreme economic losses exceeding approximately €1.02 Trillion per year (Hallegatte, et al., 2013) and the value of infrastructure and resources likely to be affected by episodic coastal flooding is projected to potentially tally up to €14.3 Trillion (Kirezci, et al., 2020). These studies provide projections based on current protection levels only and without either coastal defence or adaption measures respectively.

With 15 out of the 20 global megacities situated in LECZs (The World Bank, 2010), it provides an insight into how significant flooding and inundation issues are on a local to global scale and the necessity of human interventions to mitigate the issue. Upgrading the coastal protection standards is a mean to sustain or decrease the risk, impact and frequency of flooding (Hallegatte, et al., 2013). Flood assessments can be deemed to be a key element in achieving targets such as the Sustainable Development Goals (SDGs) Clean water and Sanitation (6): Industry, Innovation and Infrastructure (9): Sustainable Cities and Communities (11): Life on Land (15). These assessments are an integration of the flooding hazard, exposure and vulnerability assessments that produces maps which can act as tools to illustrate these components (Dastgheib, 2022). Full comprehension of the risks via these assessments can allow various stakeholders to make appropriate decisions in terms of but not limited to, adaptation, mitigation or acceptance concerning the said risks (EXCIMAP, 2007). This is critical as limited protection measures leads to higher socio-economic impacts due to flooding, while investments in unnecessary means of protection leads to wastage of finances which is also undesirable (The World Bank, 2016).

This research will focus on the hazard assessment component with a focus on coastal flooding and the indicator as flooding extent and depths. SFINCS, a reduced-physics solver that is capable of compound coastal flooding computations (Leijnse, et al., 2021), would be utilized to develop a methodology in deriving coastal flooding extents and depths on a continental scale. Literature that addresses the impact of coastal inundation on such a large scale is very limited, leading to a lack of information and the ability to predict such events (Vousdoukas, et al., 2016). Static inundation approaches have been explored in the past (Hinkel, et al., 2014, Hinkel, et al., 2010) that ignores critical contributors to the ESLs, and intermediate plus full-physics process-based approaches have been evaluated by Vousdoukas, et al. (2016) neglecting the CC scenarios. The intended research will attempt to explore the application of SFINCS

solver in hazard assessments, particularly on flood mapping on a continental scale, with consideration given to ESLs. This application of SFINCS can contribute to decision making and scientific research by providing an approach that produces fast results due to lower computational demand and is still relatively accurate for the intended flooding simulations and maps.

1.3 Novelty and Practical Value

Flood hazard assessments on a continental to global scale have become common practice but analyses of particularly coastal flood hazards on such a scale are not as frequent or advanced in comparison to river flooding events (Paprotny, et al., 2018). Paprotny, et al. (2018) also highlighted that with the increased emphasis on CC driven changes such as variation in storms and sea levels, comprehensive and accurate coastal flood hazard assessments on global or continental scales that consider these factors would be necessary. Flood maps are a crucial component in flood management and reliable maps can help professionals in the field and decision-makers to identify hotspots and plan strategies or policies accordingly in those locations (Albano, et al., 2018).

SFINCS solver has the potential to contribute significantly in this context and be an innovative solution to simulate compound effects in coastal flooding. Leijnse, et al. (2021) established that this relatively new reduced-physics solver can compute the applicable coastal processes for compound flooding at a faster rate than conventional process-based models such as Delft3D or Xbeach and is comparable in accuracy unlike simple static models. Eilander, et al. (2022) highlighted the requirement for global scale compound flood hazard modelling and developed a framework for it. The framework included a local scale SFINCS model for flooding, with an automated model setup from global datasets coupled with relevant global models. This framework was deemed a promising advancement in this field due to its automation, replicability and global application. Implementing this framework to a continental to global flood model could be the next plausible step.

Another intermediate solver, LISFLOOD-AC (LAC) has been previously used to simulate flooding on a continental and global scale (Vousdoukas, et al., 2018b, Vousdoukas, et al., 2016). A limitation of this model is that wave-driven processes such as wave breaking, setup and runup are not represented by this model (Leijnse, 2018). LAC runs on a 1-dimensional inertial model where advection is neglected and also factors such as wind-induced setup cannot be represented in the model (Bootsma, 2022). SFINCS is capable of representing these relevant processes adequately and therefore, has the potential to estimate flooding events more accurately than LAC, given that it can successfully be applied on a similar scale. Details of SFINCS is further discussed in chapter 2.

The novelty of this research is to explore the application of a flood model on a continental scale using SFINCS, considering the ESL input and spatial extent. Simulations for ESL return periods on separate segments of the total domain would need to be conducted for producing informative flood maps with acceptable accuracy. This would be one of the earlier attempts to check whether the SFINCS solver is computationally feasible and sufficiently accurate for a large-scale model as it has previously been successfully applied at a local scale in various researches (Leijnse, et al., 2021, Parodi, et al., 2020, Sebastian, et al., 2021). Subsequently, the intention is to provide a useful contribution within the hazard assessment field that can be further developed and upgraded to be utilized in extensive flood risk assessments for research or decision-making purposes.

1.4 Problem Statement

Estimating the impact of coastal floods as a hazard with influence from natural climate variability or anthropogenic climate change is critical for the people that resides in these coastal regions and are vulnerable to the threat of flooding events. It is important to understand and identify the extent of this threat with regards to the direct implications on human lives, socioeconomic impacts and the potential degradation of the natural environment.

Better understanding of the potential coastal flooding events would allow for better preparation and response measures to be put in place, such as flood protection structures, emergency procedures, evacuation plans and more. Coastal regions usually rely heavily on tourism and fishing industries, where flooding events can have significant economic impacts on the communities. Also, properties in these regions are of higher value, as it is often considered a more desirable area to live, given the scenic views and lifestyle. Hence, damage to these properties and infrastructure can result in greater loss of income for these regions, which should be considered. These regions are also potentially rich in coastal ecosystems, resulting in severe environmental impacts due to flooding which is linked to the socioeconomic factors. Environment and socioeconomic levels are closely intertwined as a healthy environment can support economic growth and social well-being of a particular region.

With these impacts in mind and considering the vulnerability of coastal regions to future climate variations, understanding the extent of potential coastal flooding can help in developing long-term adaptation strategies and reducing the risk of damage. As previously highlighted, large-scale evaluation of coastal flooding estimates as a hazard with regards to risk assessment is not common (Vousdoukas, et al., 2018c, Vousdoukas, et al., 2016) With the significance of the flood hazard expected in the future, reliable flood estimates at a large-scale can be considered crucial in tackling these issues. The reduced physics solver SFINCS, can be a tool that can be immensely useful, given its low computational expense with sufficient accuracy. It is not deemed to be a replacement for full physics models such as Delft-3D, but a rapid scan tool for larger domains and various scenarios the user is trying to model (Goede, et al., 2022). The primary goal of the research is to assess the potential utilization of SFINCS for this purpose in the future on a large-scale.

1.5 Research Objectives

With the problem statement in mind, the main and sub objectives for this thesis are presented below:

Main Objective:

Develop a methodology to model and estimate the extent of coastal flooding due to extreme sea levels on a continental scale by utilizing the reduced-physics solver SFINCS.

Sub-objectives:

- Expand the applicability of the SFINCS solver to a continental scale and produce viable estimates for coastal flooding impacts within Europe
- Investigate the current limitations and potential developments to the SFINCS solver
- Compare with other available flood model results in literature for verification.

1.6 Research Approach

The goal of the study is to attempt to utilize the reduced-physics solver SFINCS in generating flood estimates based on ESLs. Methodology is to be developed where the solver can be applied on a large-scale to obtain flood depths and flood extents. The approach strives to answer the research questions given below:

Main Question:

How to apply SFINCS solver on a continental scale and determine to what extent it can be considered a viable option in terms of computational efficiency and reliability on this scale in estimating coastal flooding impacts for extreme sea levels?

Sub-question:

- What are the current limitations and possible developments that can be associated with the SFINCS solver to carry out the large-scale assessment?
- How does the results from SFINCS compare with earlier studies conducted on a similar scale?

1.7 Thesis Chapter Outline

The layout for this thesis report is as follows. This chapter, Chapter 1 introduces the research background, motivation and significance, problem statement and the objectives of the research. This is followed by the literature review and further context to the research in Chapter 2. Chapter 3 presents the methodology developed and adopted to investigate solutions to the research questions previously outlines. Chapter 4 contains the results and its analysis obtained from implementing the methodology. The significance of the results is also discussed within this chapter which aids in answering the research questions posed and determine whether the research objectives were achieved. This chapter also discusses the limitations of the study and further research recommendations and identified gaps that could be filled in the future.

Appendices – Additional material that supplements the thesis:

A. Research Ethics Declaration Form

B. Research Ethics Personal Statement

C. SFINCS Equations

D. Information on the Model Setup Scripts

Chapter 2 Literature Review

To help establish the context for the research, identify research gaps and build a foundation for new research, this chapter includes relevant information regarding the thesis topic. The literature review follows from the previous introductory chapter and comprises of a summary of hazard estimation, computation of extreme sea levels, current flood model approaches and uncertainties involved in it. Together with a discussion on these topics, comparison of relevant solvers is presented along with details of the SFINCS solver that is utilized in this research.

2.1 Hazard Estimation in Risk Assessment

Risk can be defined as the potential for repercussions where a valuable asset is endangered and the outcome or conclusion is unknown considering a possible range of values (IPCC, 2014). It is often described as the product of probability of an event or trend occurring and their impacts. Risk assessment is the quantitative or qualitative estimation of risk, required for better risk and resource managements. Various stakeholders or decision makers need risk assessment data for risk informed decision making to incorporate appropriate mitigation or adaptation strategies in their policies and infrastructure planning (Dastgheib, 2022).

According to IPCC (2014), three components of risk assessment are identified, which is Hazard, Exposure and Vulnerability. A brief description of these components based on IPCC (2014) is given below:

- **Hazard**: refers to the potential occurrence of a climate-related event, such as a flood, heatwave, or drought. The event could be natural or anthropogenic and results in detrimental effects on its subject matter.
- **Exposure**: refers to the account of human or natural systems present in a certain location facing the climate-related hazard. For example, exposure to a flood hazard may depend on factors such as population density, infrastructure, ecosystems, land use patterns and various assets that could be negatively affected.
- **Vulnerability**: refers to the degree to which human or natural systems are susceptible to harm from exposure to a climate-related hazard. Vulnerability is influenced by factors such as socioeconomic status, age, health, and access to resources, and can vary widely across different populations and locations.

These three risk assessment components, when combined, provide a framework for understanding and assessing the possible implications of climate-related disasters on human and environmental systems. Policymakers, planners, and communities may establish suitable measures to mitigate the risks associated with climate change and increase resilience to its consequences by assessing each component and their interrelationships. Such assessments can assist policymakers in identifying flood-prone locations, prioritizing flood mitigation resources, and developing effective flood management strategies. Following are some instances of how flood risk assessments might help policymakers:

- Long-term infrastructure development strategies and adaptation planning (Hinkel, et al., 2021).
- Zoning decisions: Flood risk assessments can help policymakers make informed decisions about where to allow infrastructure development and where to restrict it based on flood risk. Porter and Demeritt (2012)elaborated on how flood maps were designed to circumvent development in flood-prone zones without outright prohibiting such developments.
- Infrastructure planning: Flood risk assessments can inform infrastructure planning decisions by identifying areas where infrastructure is most vulnerable to flood damage. For example, a flood risk assessment might identify critical roads, bridges, or other infrastructure that require additional flood protection.
- Emergency planning: Flood risk assessments can also inform emergency planning decisions by identifying areas that are most at risk during a flood event. For example, policymakers can use flood risk assessments to identify areas where evacuation routes are needed or where emergency shelters should be located.
- Aid organizations such as United Nations Office for Disaster Risk Reduction in bringing together different stakeholders, such as governments and communities, to decrease the risk of flooding catastrophes and losses (UNDRR, n.d.). This helps create a safer, more sustainable future.

As highlighted, risk assessments are critical for proper planning and expenditure of limited resources. As adequate hazard estimation on larger scales is a prerequisite for broad risk assessments, an improved comprehension of the flooding hazard details, including an enhanced knowledge of the costs associated with the hazards and disasters is required for detailed risk assessments and prudent investments in mitigation and adaptation (The H. John Heinz III Center for Science, 2000).

2.2 Relevant Processes for Extreme Sea Levels and Coastal Inundation

As highlighted before, ESLs leading to coastal flooding and inundation is the focus of this research in terms of boundary conditions. To attempt to model this, it is necessary to have a clear understanding of what ESL is and how it is defined. ESL is a result of a meteorological conditions such as storm surges combined with atypical tide levels, with the influence of RSLC (Gregory, et al., 2019). Episodic forcing components such a storm surges and wave setup are critical in terms of their influence on extreme sea levels which could also potentially result in coastal flooding (Muis, et al., 2016, Vitousek, et al., 2017). When these storm surges coexist with elevated water levels due to tides, such as the occurrence of spring tide, the coastal flooding extent escalates immensely (Leijnse, 2018). These water levels are generally combined via equations to represent the factors in a model. Two approaches in representing ESLs from recent literature are given below:

Table 1: ESL formulations in relevant literature

Equation	Details	Author
$\boldsymbol{ESL = MSL + \eta_{tide} + \eta_{CE}}$ $\eta_{CE} = \eta_{storm\ surge + 0.2.H_s}$ **(Non-stationary approach)**	η_{tide} = *high tide water level* η_{CE} = *water level fluctuations due to climate extremes* For the η_{CE}, present values are obtained from a global reanalysis and future values are obtained from a 6-member Global Climate Model ensemble. Probabilistic process-based method for the calculation of regional SLR projections (RCP 4.5 & 8.5) and the effect of RSLR with multiple boundary MSL conditions were considered for η_{tide}. Probabilistic projections of ESLs were generated using probability density functions (PDFs) of η_{CE} , η_{tide}, RSLR and combining them by utilizing Monte Carlo (MC) simulations.	(Vousdoukas, et al., 2018a)
$\boldsymbol{TSL(t) = T + S + WS}$ $\boldsymbol{Future\ ESL = TSL + RSLR}$ **(Stationary approach)**	*T = tide, S = Storm Surge, WS = Wave Setup* Historical total sea level (TSL) estimates validated against extensive global tide gauge data. Statistical extreme values were obtained. Extreme estimates of TSL is then linearly added to Projected regional RSLR from RCPs 4.5 and 8.5 to get future ESL values	(Kirezci, et al., 2020)

Kirezci, et al. (2020) demonstrated that tides and storm surges remain the governing components in global flooding extents and RSLR causes notably more frequent coastal flooding events. Hence for a continent scale coastal flooding research, inclusion of these aforementioned components to represent the ESLs in the model is critical. For the purposes of this research, to emulate extreme sea levels as boundary conditions, ESL data from Vousdoukas et al. (2018a) was utilized. How these levels were implemented within the model is further discussed in the relevant Methodology section.

2.3 Flood Model Approaches and Uncertainties

A lack of research on coastal flood mapping, particularly on a continental to global scale has previously been brought. It is a complicated process with the involvement of multiple significant processes that is to be implemented at various time and spatial scales. From literature, it can be deemed that there are three general approaches to simulate the intended flooding events. These are simple static, intermediate reduced-physics and full process-based models or approaches.

Considering the classic bathtub approach or planar surface projection method for the static model, this approach basically compares the input forcing water levels and the elevations. If the extreme water levels exceed the input Digital Elevation Model (DEM), these particular areas result in inundation (Vousdoukas, et al., 2016). This non-process-based model is very fast, making it appealing for large-scale applications (e.g. Kirezci, et al., 2020). However there appears to be many limitations of this approach which is reflected in the literature. Significant overestimation of the flood extent has been reported compared to hydraulic models (Bootsma, 2022, Breilh, et al., 2013, Vousdoukas, et al., 2016)

With the lack of representation of hydraulic processes in the model, temporal variations in storm surges, tidal levels and waves cannot be simulated with the static approach. Furthermore, accurate predictions in low elevation areas are not achieved due to lack of landscape roughness effects (Ramirez, et al., 2016). Considering these limitations together with the current availability of computational capacity, more dynamic modelling approaches are adopted over the static ones (Leijnse, 2018).

The diametrical opposite of static approaches is the advanced full-physics process-based models. These models can represent the full range of hydrodynamic processes influencing the flood extent. Large-scale shallow water equation (SWE) models such as Delft3D-FLOW (Lesser, et al., 2004) and MIKE (Warren and Bach, 1992), plus non-hydrostatic SWE models (NHSWE) on a smaller spatial scale such as SWASH (Zijlema, et al., 2011) and Xbeach-nh (Roelvink, et al., 2018) are potential options available to simulate the key processes. However, the drawbacks of these models are that they are computationally expensive, rendering them ineffective for large-scale simulations and probabilistic approaches (Vousdoukas, et al., 2016). Furthermore, Vousdoukas, et al. (2016) also highlights that the limited availability of high-resolution topography data that is required for such models is also a constraint for the application of these models.

The compromise between these two are the so-called intermediate approaches or solutions. They are meant to utilize simplified equations with adequate accuracy and is computationally inexpensive (Leijnse, et al., 2021). Vousdoukas, et al. (2016) tested an intermediate approach for coastal flooding using LAC (Bates, et al., 2010), a 2D hydraulic model that is part of the dynamic reduced complexity model LISFLOOD-FP (LFP). Originally intended for river flow and subsequent floodplain inundation modelling, Vousdoukas, et al. (2016) recognized its potential for large-scale coast flood simulations given the success in global scale river flood mapping efforts and simulating coastal related events such as storm surges and SLR.

This study also had it limitations. Vousdoukas, et al. (2016) highlighted that adequate DEM resolution is critical for inundation models, but they are not readily available to run a model on a continental scale and high resolutions would lead to unacceptable computational costs. A 100-metre resolution DEM was eventually utilized and was deemed to be too coarse to incorporate coastal protection structures, for which information is again lacking as thorough information regarding the European flood protection structures are scarce (Scussolini, et al., 2016).

Vousdoukas, et al. (2016) compiled flood protection data via open databases and personal communication with coastal field personnel and national authorities. Where no relevant information was available, an assumption of minimum protection standard implementation was adopted by the authors based on the population density. Also, CC driven variations were not part of this particular study. Kirezci, et al. (2020) also ran flooding simulations at a global scale with no flood protection input. Over-estimation of the flooding event was an accepted consequence and it was concluded that absolute flood extent values are not very useful in these cases. A considerable number of global datasets were combined to extract global projections for ESLs and subsequent flooding extents and flood depths in the future. This also brings in uncertainties to the model as they are already present within the RCP scenario data from GCMs. The statistical uncertainties in both ESL and RSLR were acknowledged and clearly quantified by Kirezci, et al. (2020).

How the extreme levels are fed to the model is also a critical aspect to focus on. Vousdoukas, et al. (2016) derived maximum tides from 10-year data analysis of a global system to derive a time series of the tidal elevation. A time series for extreme storm surge levels was obtained from a storm surge hindcast run and the time series of significant wave height (H_s) from ERA-INTERIM dataset (Dee, et al., 2011). With the lack of nearshore bathymetry at the continental level, the two-time series were combined to get the extreme water levels for the model via an approximation of the wave setup that was adopted from United States Army Corps of Engineers (2002). This was followed by an extreme value statistical analysis (EVA) to get the time series for the total water levels considered by the authors. To incorporate the temporal component of the extreme events which the EVA lacks, design hydrographs (Cialone and Amein, 1993) were utilized. Extreme events from the combined time series of waves and storm surges were recognized and for each event the peak water level and duration were approximated. Design hydrographs are then created considering a best linear fit relationship between peak water levels and duration of events.

Statistical models that incorporate PDFs for various components are probabilistic models where the exact relationship between quantities is not known, which is the opposite of a deterministic model (Rey, 2015). Vousdoukas, et al. (2018a) dealt with the temporal component of the LAC model by performing a MC analysis consisting of PDFs for contribution of storm surges plus waves, high tide water levels and RSLR. This is elaborated further in Figure 2.1 given below. Same wave setup approximation as mentioned before was utilized and the corresponding MC simulations results in a synthetic triangular hydrograph that is applied at model source points along the coast.

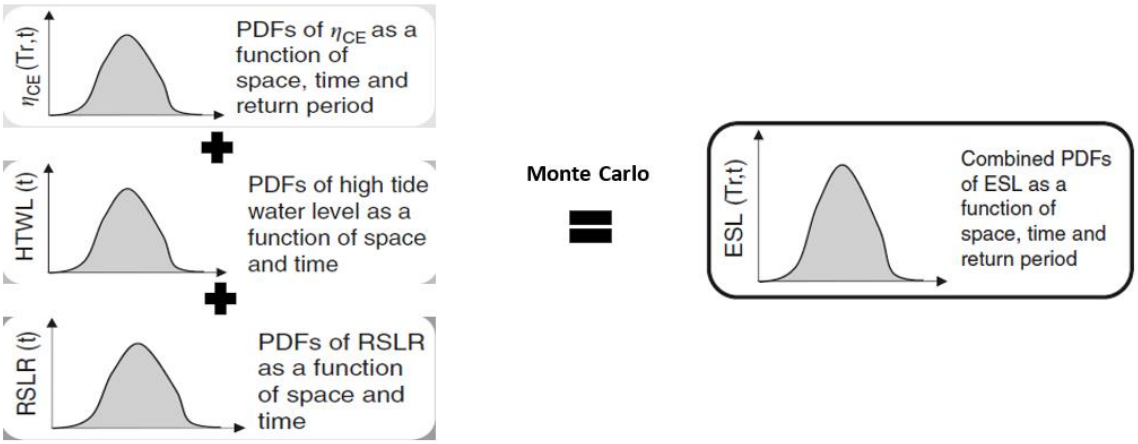

Figure 1: Procedure to generate ESL projections (Vousdoukas et al., 2018a)

Kirezci, et al. (2020) who performed a bathtub analysis, obtained the wave setup using the SPM graphical approach (United States Army Corps of Engineers, 1984) and parametrization given by Stockdon, et al. (2006). The episodic coastal flooding extremes were predicted by fitting a PDF to a historical time series. Peak over Threshold approach was adopted after testing various methodologies which included alternatives such as Annual Maxima (AM) and the use of a MC approach. Flood hazard modelling generally follows a probabilistic approach to account for forcing uncertainty and help stakeholders to make risk-based decisions (Ranasinghe, 2022).

2.4 Background on SFINCS

Developed by Deltares, SFINCS is a process-based reduced-physics solver that is considered computationally efficient (Leijnse, et al., 2021). Based on the LFP model (Bates, et al., 2010), the intended use of the solver was simulating compound flooding events in coastal zones. The speed and the ability to be applicable for domains extending to thousands of kilometres, make this computationally economical solver a prime candidate to carry out fast hazard assessments resulting from ESLs on a continental scale. Also, the ability to apply different forcing such as wave processes, discharges, wind and precipitation, leads to SFINCS being an appropriate solver for flooding and inundation applications. LAC, another popular intermediate solver that has been mentioned in the earlier sections, is limited to just modelling river discharge in terms of compound flooding (Leijnse, et al., 2021). Its lack of representation of waves in the model for example, limits the use of the solver in coastal flood modelling as processes such as wave runup cannot be modelled.

SFINCS obtains its computational efficiency by numerically solving only the necessary processes of compound flooding in an straightforward and quick manner (Leijnse, et al., 2021). The solver is based on simplified Saint-Venant equations and governed by the momentum and continuity equations where the three unknowns, water level (ζ) and momentum fluxes in both x plus y directions (q_x and q_y) are solved. Saint-Venant equations are shallow water equations in one directional form that have been obtained from depth-integrating the Navier Stokes (NS) equations. The simplifications only consider momentum and continuity resulting from bed-level gradients plus local friction with the addition of water level to the pressure gradient term. The model can resolve the local inertia equations (LIE) and simplified shallow water equations (SSWE) with the addition of local acceleration and advection respectively (Leijnse, et al., 2021). Components making up the full shallow water equations (SWE) such as, Coriolis, viscosity and atmospheric forcing terms are neglected. As for the numerical grid, SFINCS implements an equidistant, rectangular version of the Arakawa C-grid, that is a staggered grid. The bed and water levels are expressed in the cell centres, while the fluxes and flow depths are resolved in cell edges.

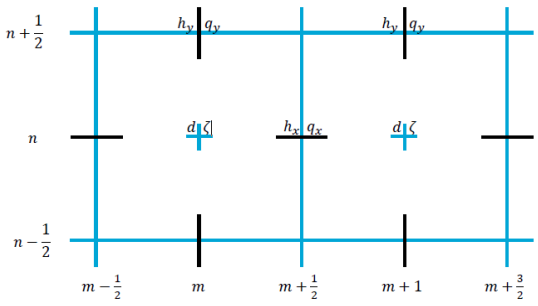

Figure 2: Numerical grid for SFINCS with relevant variables (Leijnse et al., 2021)

Water depths computed at the cell edges decides the wet and dry cells for the flooding and drying mechanics based on a threshold depth (Leijnse, 2018). Advection and momentum fluxes

to the dry cells are prevented by this threshold limit. For both momentum equations, an explicit scheme is utilized that have been smoothed further by a Lax-scheme for increased stabilization of the numerical solution (Leijnse, 2018). The 1D and 2D advection terms are incorporated using the Upwind and Central Difference schemes respectively, and calculating water levels via the continuity equation follows the BTCS scheme (Leijnse, 2018). Stability of this numerical scheme in SFINCS is established by the CFL condition and subsequently setting a time step value Δt using the equation 2.1 given below:

$$\Delta t = \alpha \frac{\Delta x}{\sqrt{g h_{max}}} \qquad (2.1)$$

In accordance with the equation, the timestep Δt is determined based on Δx and hmax, that is the maximum magnitude of water depth over the domain that is being computed (Leijnse, et al., 2021). To achieve and enhance the stability of the model, a heuristic time step reduction factor (α) is also often implemented. Ranging from 0.1 to 1 with the default value is set at 0.75, this factor is utilized to ensure model stability (Leijnse, et al., 2021, Leijnse, 2018). A full set of relevant equations represented in SFINCS is presented in Appendix B.

Leijnse (2018) performed and assessed multiple conceptual tests and case studies to investigate the performance of SFINCS. It was highlighted that SFINCS does not resolve the processes within the surf zone such as wave breaking or wave setup, and wave-directions are also not accounted for in the model. Hence, the user of the solver is required to apply a time series at rapidly and slowly varying water levels on the seaward boundary of the swash zone which is to be acquired from either phase resolving models or large-scale circulation models. Leijnse, et al. (2021) also points out that SFINCS can generate time series for the aforementioned water levels at the boundary with the aid of empirical relations. These relations give input values for the wave setup and height as a function of the offshore conditions and surf zone bed slope.

Leijnse (2018) concluded that the advection term and the inclusion of incident waves as part of the incoming waves spectrum is necessary to model wave runup adequately. It was also highlighted that the absence of a non-hydrostatic term is a deficiency of the solver in estimating runup. For the case study of compound flooding in Jacksonville, it was concluded that SFINCS is adequate in simulating all the relevant main hydrodynamic processes and the simplified model has no notable effects on the results. For the case study of town Hernani, the magnitude of flooding was considered to be underestimated and inclusion of the advection term gave more realistic results in terms of the overtopping flow of water.

Sebastian, et al. (2021) performed a hindcast of Hurricane Harvey using SFINCS solver and obtained results comparable to the observed data, deeming the model to be sufficient quality. Furthermore, Parodi, et al. (2020) successfully utilized SFINCS to produce flood maps for better understanding input uncertainties in coastal flood risks for small island developing states. This thesis attempts to develop a methodology to apply the SFINCS model on a continental scale, which is still not widely used in the current early stages of SFINCS development. A computationally efficient model or approach such as SFINCS would immensely help in generating flood information on a continental scale with reduced computation expense.

2.5 SFINCS and other Flood Modelling Solvers

Coastal flood modelling on a larger scale such as the global scale, has been implemented by various studies in the past. The most commonly assessed methodology has been based on the aforementioned classic bathtub approach or planar surface projection method. The assumption is that all areas with a lower elevation level than the input water levels at the boundary conditions that are hydrologically linked to the ocean undergo flooding. As previously highlighted the popularity of this methodology, particularly considering the magnitude of the scale is primarily to due lack of computational costs and size, plus limitations in the inputs of the model such as high-resolution elevation data (Ramirez, et al., 2016). The lack of hydrodynamic process in these continental to global scale flood models results in potentially unrealistic water depths and flood extents in terms of their large magnitudes (Vafeidis, et al., 2019). Lack of consideration to the hydrodynamic processes in these models, such as effects of surface roughness are areas where potential improvements can be made to obtain better results in the stage of hazard estimation (Vafeidis, et al., 2019).

This bathtub approach or Graphical Information System (GIS) based inundation approach has been subjected to model modification factors to obtain better results. Vafeidis, et al. (2019) explored the utilization of probable water-level attenuation values that are available to account for the attenuation due to surface roughness. Tiggeloven, et al. (2020) included three factors that are not commonly considered in such inundation models. As tides and storm surges have a finite time duration, a resistance factor was utilized to model the decrease of flooded land as the water progresses similar to attenuation factors by Vafeidis, et al. (2019). This resistance factor was also weighted proportionate to the quantity of permanent water in each cell, accurately approximating them as low resistance cells. Lastly, a spatially changing offset between the MSL and the terrain model was implemented to guarantee that the zero datum of the terrain and the ESLs are consistent. Implementation of such factors most likely would improve the results of this flooding model approach, but still leaves potential gaps that could be addressed using intermediate solvers. Results from Tiggeloven, et al. (2020) was utilized to do a comparative analysis for this study and is presented in Chapter 4.

Ramirez, et al. (2016) used a dynamic reduced-complexity (DRC) model to simulate storm tide flooding. The DRC model utilized the CAESAR-Lisflood solver that solves the SWE without considering the advection term. The study successfully implemented the DRC model on a spatial resolution of 90 m within a regional scale. Lewis, et al. (2013) utilized LFP with Shuttle Radar Topography (SRTM) terrain data to run a dynamic coastal inundation model in the northern Bay of Bengal. These studies at national levels have led to the implementation of intermediate solvers on larger scales such as Vousdoukas, et al. (2016) and Vousdoukas, et al. (2018c) using LAC on a continental scale to produce inundation extents. Application of SFINCS on a national to continental scale, could potentially lead it to be an alternate to LAC in inundation modelling with more input parameters available for the user to simulate the flooding conditions.

Both SFINCS and LAC are based on the LFP model (Bates, et al., 2010). Although there are some differences in their features and the range of input parameters and processes. SFINCS is based on rectilinear grids and LAC uses rectangular grids (Leijnse, 2020). Rectilinear grids are created by dividing a physical domain into a series of grid cells that have sides parallel to the coordinate axes, but the grid spacing in each coordinate direction may vary. This means that

the grid lines are not necessarily straight lines, but they still remain parallel to the coordinate axes. The grid spacing can vary along each direction, which makes it possible to have a non-uniform grid spacing in a specific direction, making it useful in cases where the physical phenomena varies greatly in that direction. Rectangular grids, on the other hand, have grid cells with sides that are straight and parallel to the coordinate axes, and the grid spacing in each coordinate direction is uniform. This results in a grid spacing that is constant in all directions, which makes the rectangular grid easy to generate and manipulate. In addition to regular grid mode, SFINCS also have a subgrid mode (Goede, et al., 2022). This is a better alternative to finer grid resolutions that can lead to longer simulation times and with the subgrid mode, the model is run on a coarser grid resolution without compromising the accuracy of the results. The subgrid mode is not implemented in this study.

Both the solvers have dimensions of 2D horizontal solving capability but in SFINCS the advection term can be included. Wave generation is not possible in both the solvers. However, SFINCS can represent wave processes, storm surges and tides via input files and have limited capability of wave resolving (Leijnse, 2018). Swash zones could also be resolved in SFINCS and Coriolis forces are neglected in both solvers, meaning the boundary conditions should be specified in close proximity to the coast. Furthermore, morphological changes cannot be simulated with either of these solvers (Leijnse, 2018).

Simple infiltration and river discharges can also be part of the input in SFINCS. A constant value throughout, spatially varying constant value or the Curve Number method can be specified as infiltration in SFINCS and could be significant when modelling with precipitation, which is also another process that could be incorporated in SFINCS but not in LAC. Past studies on LFP generally concludes that if the flow is subcritical and the variation is not rapid, the inertial equations approximate the full SWE quite well. SFINCS with its flexibility in various inputs, the inclusion of the advection term and the option for different grid modes, can potentially prove to be a more capable alternate to LAC in coastal inundation modelling.

Some of the disadvantages in the Lisflood models include the inability to create flexible cell sizes. Hence the magnitude of cells needed to generate accurate results could be increased which directly effects the computation efficiency of the solver negatively. Also, solely considering the water height in the weir overflow equation could be a problem for storm surges and the lack of error warnings in the solver can cause major issues to the user (Peterse, 2016). If the user makes a mistake in one of the control parameters, which is easy to do, this control parameter is disregarded rather than the program providing feedback on this unrecognized control parameter. This might cause major issues in interpreting data and handling errors.

Hazard refers to the potential occurrence of a natural or anthropogenic event such as flooding and is the first of three components for risk assessments, other being Exposure and Vulnerability. As risk assessments are critical for understanding the risks we face and plan strategies for it, obtaining proper hazard estimates are a key prerequisite in undertaking these assessments.

A computationally efficient dynamic modelling approach replacing the traditional Bathtub approach and other inefficient or unreliable models, in large-scale flood estimation would greatly aid in this objective. The reduced-physics solver SFINCS, which is based on the LFP model can be a potential intermediate model for this purpose. SFINCS has the capability to numerically solve processes of compound flooding in a simplified and fast manner. ESLs, which are a result of meteorological conditions such as storm surges, tide levels and relative sea level rise, can be fed to this solver to simulate coastal flooding and inundation. This is the methodology adopted for this study.

Considering the uncertainties in large-scale flood modelling such as, application of boundary conditions, lack of information on flood protection structures and limited elevation data resolution, there are gaps identified in accurate flood estimate studies and the development of a methodology utilizing a solver such as SFINCS to study these further, can be very beneficial in this sector.

Chapter 3 Methodology

This chapter describes the methods used in this thesis to obtain the results which is presented in Chapter 4. Knowledge from the literature research on SFINCS is utilized to formulate a methodology to apply the solver on a larger scale and details of the setup are outlined in this chapter.

3.1 General Approach

The general approach followed during the thesis is outlined in the flowchart below. The primary focus of the research and its methodology was to setup the SFINCS model with regards to generating the necessary inputs required to run the simulations. The subsections of this chapter will go through in details how the model setup was conducted and elaborate on how it could be potentially used or adopted in future SFINCS research attempts.

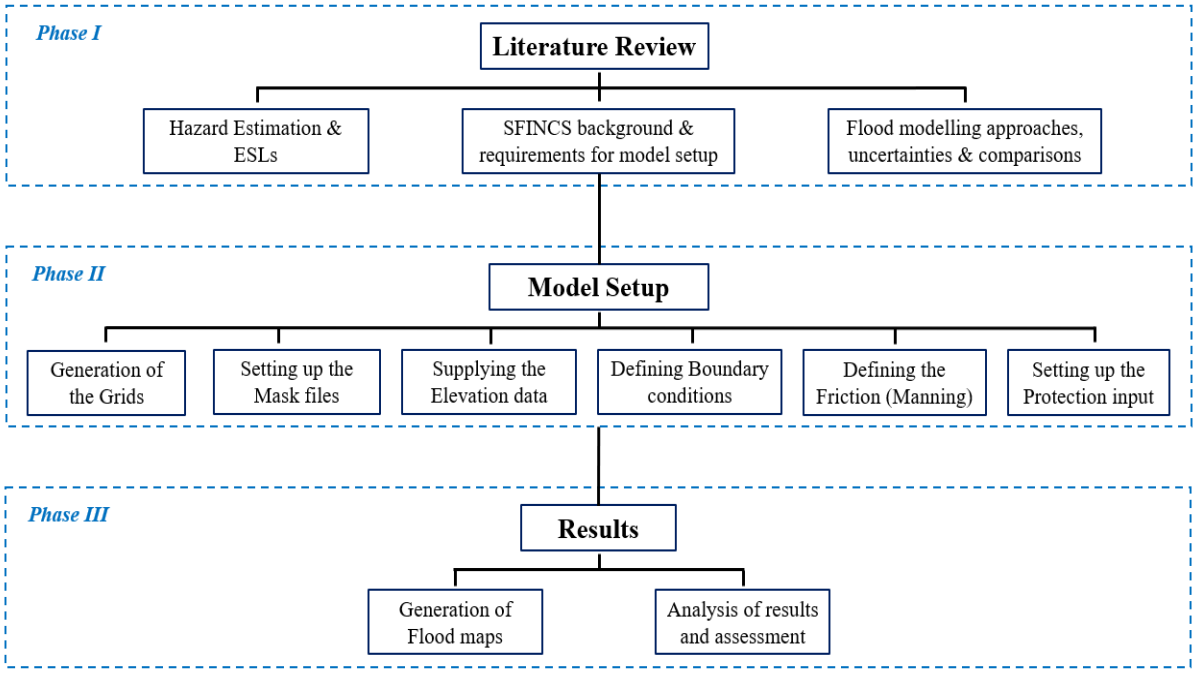

Figure 3: Flowchart with the phases of the research methodology

All the Matrix Laboratory (MATLAB) scripts produced and additional supporting functions in relation to this methodology are available online and the details are presented in Appendix D for reference.

3.2 Generation of the Grids

The details of the grid implemented in SFINCS has previously been discussed in Section 2.4. As for the input to the SFINCS model, the grid characteristics have to be defined in the main "sfincs.inp" file. Seven properties of the grid are required to be outlined in the input file and they are as follows:

- Origin coordinates of the grid. This is the bottom left corner of the grid defined by an x0, y0 coordinate that can exclusively be in cartesian coordinates. This is a requirement for the SFINCS model (Deltares, 2022).
- Amount of grid cells in both X and Y direction which is labelled as mmax and nmax respectively.
- Grid sizes in both X and Y directions labelled as dx and dy respectively.
- Rotation with the magnitude in degrees and anti-clockwise from the horizontal x-axis.

For the application of the solver on a large-scale, a methodology needed to be developed to automate the process of creating grid inputs to a certain extent. The generation of the grid parameters considering the coastline, orientation of land to sea, adequate coverage inland within the grid and overlapping of the grid, was done using Quantum Geographic Information System (QGIS) and MATLAB. Taking into account the scale and the automation process, a uniform grid size of approximately 100km by 100km was adopted to keep the process relatively simple, with the amount of grid cells in both directions equalling 3333 and with the resolution set at 30 metres. This is consistent with the DEM data that was utilized and will be further discussed in Section 3.3. Details of the procedure developed to obtain the grid characteristics are outlined below:

- The boundary of the coastline via shapefiles was obtained online or using the Delft Dashboard. Using polygons, the coastline required can be extracted within Delft Dashboard as a land boundary file.
- To deal with land boundary files, they were loaded to the "lbdTool" which is part of the Open Earth Tools (OET) that can be opened via MATLAB. A coarser scale such as 1:114872 was used to extract the coastline via Delft Dashboard to eliminate the small offshore island boundaries for simplicity.
- From the "lbdTool", the land boundary was exported as a shape file which was then loaded onto QGIS.
- First step in QGIS was to use the "Reproject layer" function from the processing toolbox as the default projection EPSG:4326 is not suitable for analysing distances such as buffers and is not a cartesian coordinate system that can be implemented in SFINCS.
- Next a buffer was created using "Single sided buffer" function in the processing toolbox and then the "Dissolve" function to combine the buffer polygons.
    - There could be polylines that still need to be eliminated. This was done by exporting the buffer as a DXF and easily deleting them in AutoCAD. It was then imported back to QGIS and saved as a shapefile.
- Next step was to create grid hook up points on the buffer layer. An initial point was created within a "single point" layer. The option "Enable snapping" should be kept on to have the point snap onto the buffer layer.
- To create grids of approximately 100km by 100km with an overlap of approximately 25km, grid hook up points needed to be within a vicinity of 75km between each other.

- A 75 km buffer was created with the “Buffer” tool around the initial point and converted to a polyline using “polygons to lines”.
- Then the new point was created using the function “Line intersections”. Any intersectional points that is not necessary was discarded.
- This created a new point in a temporary layer and the process continued until sufficient grid hook up points are created along the extent of the coastline boundary that is required. This process can be a tedious, so the QGIS model builder function was used to automate the generation of the points to save time.
- Finally, all the points were combined in one vector layer and the X/Y field was added to the layer using the processing toolbox.
- The vector layer was then exported as a CSV file and any unnecessary columns were deleted. Finally, the user has a CSV file with the X and Y coordinates of the grid hook up points that is to be further processed to create the “sfincs.inp” file.

- For the steps that followed, a switch to MATLAB was required with utilization of the necessary scripts. The first step was to determine the orientation of the grid points with relation to the coastline.
  - The grid hook up points created within QGIS and the shapefile of the respective coastlines that is being processed was loaded to MATLAB. The function “m_shaperead” (Pawlowicz, 2018) was used to read the coastline of the model location.
  - The “shapefile.ncst” data was then stored in two variables for the X and Y coordinates of the coastline. With the coastlines potentially having multiple segments due to the presence of small offshore land areas, NaN values were concatenated between the segments and then the X and Y coordinates were concatenated for all segments within a FOR loop. Otherwise unnecessary polylines could be formed between points that does not represent the actual coastline.
  - . function (Yoshpe, 2023) was then implemented to find the relationship between the grid hook up points and the coastline. The output of this function provides the X and Y coordinates of the closest points to the coastline polyline.
  - This was then used to find the distance between the points and the function “atan2d” was used to find the angle between the distance vector and the x-axis in degrees. The angle was measured in anti-clockwise direction and this angle was then used to classify the grid point between one of four quadrants:

    - Quadrant 1: between 45 degrees & 135 degrees (land northwards)
    - Quadrant 2: between 45 degrees and 315 degrees (land is eastwards)
    - Quadrant 3: between 225 degrees and 315 degrees (land is southwards)
    - Quadrant 4: between 135 degrees and 225 degrees (land westwards)

  - The script produces a CSV file that contains the orientation for the hook up points, but this orientation might still not be fully accurate. This is due to the non-uniform nature of coastlines which leads to the output of undesired orientations relative to the side of the land the point lies on. A separate excel sheet was then used to manually fix the orientation based on the visual assessment of point locations on the map. The developed script does the plotting too for this purpose.
- Next step in the methodology was to potentially adjust the grid points based on the coastline with minimal manual intervention. This can be labelled as a built-in check for

the points to ensure that all of the land area is within the grid and no boundary points are excluded from the model grid. The rectangular grids generated from the grid points should not exclude any extent of the coastline.
    - This check was conducted using horizontal and vertical check polylines. If the vertical or horizontal check vectors intersect with the buffer polyline, then it indicates that the grid point should be displaced or relocated further away from the coastline.
    - An IF condition and the "repelem" function was utilized to create the check polylines based on the orientation assigned to the point. Points that are labelled for Quadrant 1 and 3 based on the orientation have horizontal check lines and the points for the other two quadrants have vertical check lines.
    - FOR loops and IF conditions were implemented to loop through all the points and if there were any intersections of the line to the coastline buffer line, the grid hook up point was moved to the maximum buffer line coordinate that is within the original grid hook up point and the intersection point. If no intersections are found, the IF condition keeps the grid hook up point at the same coordinates for extraction later.
    - These computations were carried out for each quadrant separately and the new grid points were generated based on indexing and extracted as a CSV file. The results and the coastline were plotted for better visualization of the outcome of the procedure.
- Next step in the process was to generate the grid information via MATLAB based on the grid points and automatically generate the "sfincs.inp" file in each SFINCS model subfolder.
- Based on the orientation of the grid points, the origin of the grid was computed within the script. As highlighted before, the origin points x0 and y0, needed to be specified in the "sfincs.inp" file. This origin point is always the bottom left corner of the grid, hence the X and Y coordinates of the grid hook up points was modified to get to this point based on its assigned orientations.
    - For example, x-coordinates of the grid hook up points in quadrant 4 needs to be subtracted by the length of the grid to get the x0 of the origin point of the grid, while the x-coordinate of the grid hook up points in quadrant 2 needs no further calculations. These computations were carefully scripted in MATLAB to create the final origin points
    - For all of the grids, the mmax and nmax was set to 3333 and the rotation at zero. The dx and dy was kept consistent throughout at 30. This resolution was a reflection on the DEMs used as highlighted earlier. The "repelem" function was used to add this information to all the grid point coordinates in order to make a single matrix with all the data for the definition of the grid characteristics
- The main folder path was then determined and the subfolders were created using the "mkdir" function with the folder names generated using the "sprintf" function
- Then text files with the name "sfincs.inp" were created using the "fopen" and "sprintf" functions within a FOR loop.
- The "fprintf" function was then used to write the necessary input details into the text file. This input information was based on the SFINCS manual (Deltares, 2022) and the format followed was directly adopted from the manual.
- Apart from the grid characteristics highlighted in this chapter, the input file also specifies the following:
    - depfile = sfincs.dep; mskfile = sfincs.msk; manningfile = sfincs.man; weirfile = sfincs.weir; indexfile = sfincs.ind

    - bndfile = sfincs.bnd; bzsfile = sfincs.bzs
    - advection = 0 (The advection is turned off for this study)
    - alpha = 0.75 (default value used)
    - huthresh = 0.05
    - theta = 0.9
    - qinf = 0
    - inputformat = bin (Used with spatially varying friction values)
    - outputformat = net
- The output time intervals were added to the "sfincs.inp" later in the process and will be further discussed in Section 3.5. This is because the output times are defined by the duration of the storms that are set up for the respective simulation.
- With this procedure, for the amount of grid hook up points that was being input, SFINCS model subfolders were automatically generated and the "sfincs.inp" files with the necessary input parameters were saved within each of those folders to run the simulations.
- Another MATLAB script that is presented within this study, was used to visualize the grid extents for further manual modifications. The four corners of the grids were defined based on its orientation and then the grids and the respective coastline is plotted for checking.
- If the grids were still not properly set up due to the non-uniformity of the coastline or other offshore complexities such as small islands, manually the X and Y coordinates of the hook up points were modified such that it was appropriate to generate the intended grids for the SFINCS models. Unfortunately, this was still a possibility and could not be fully avoided in this proposed automated process. Particularly for a complex coastline such as the Europe the chances are quite high for the need of manual corrections at the end of the process.
- When all the grids were set to satisfactory locations for the models a grid bounding box matrix was created with the 4 four corners and the orientation of the grid. This information was then saved as a CSV file and saved as a MAT file in each respective subfolder of SFINCS model specifying the grid information for that particular model grid.
- This bounding box information would later be loaded to MATLAB and utilized in processing other necessary inputs, so this step was for user convenience.

It is also important to highlight that the function "natsortfiles" (Stephen23, 2023) was used in this procedure and the upcoming procedures given below, to sort the subfolders of the SFINCS models alphanumerically before looping over them.

3.3 Setting up the Mask Files

Mask files are a mandatory input file in a SFINCS model to differentiate specific roles of the grid cells in a simulation. This leads to the user achieving more flexibility with improving the model domain and subsequently decreasing the simulation duration as well (Deltares, 2022). There are 4 options that a grid cell can be tagged with using the mask file. They are:

- Inactive cells with a mask value equal to 0
- Active cells with a mask value equal to 1
- Boundary cells with a mask value equal to 2
- Outflow boundary cells with a mask value equal to 3

For this study the active cells were considered to be the grid cells that fall within the buffer created from the land boundary file for the respective areas that fall within the domain. The inactive cells were then the offshore grid cells which consists of no relevant elevation data and is not needed for the output as there would be no flux calculations in those cells. The boundary conditions which consists of the water-level time series and is further discussed in Section 3.5, by principle were forced within the model only at grid cells that have a value of two. For each grid cell with the value two, an interpolated weighted average between the two closest boundary forcing input locations is computed by SFINCS. This was the locations of the ESL data points with the water-level time-series being the synthetic hydrographs derived from them and is further elaborated in Section 3.5.

The outflow boundary cells are necessary within the grid to prevent accumulation of water at the edge of the grids or adjacent to the lateral model boundaries with active grid cells. Without the outflow cells defined, the output produced has the potential to inflate the flooding results in terms of water depth obtained. Hence outflow boundary cells and the boundary cells were needed to be defined for the SFINCS model based on the grid, land area and the identified active cells. The “sfincs.msk” input files for all the SFINCS models were generated using MATLAB and the process is given below:

- The relevant buffer shapefile that is to be used to identify the active cells of the grid was loaded to MATLAB using the function “m_shaperead”.
- A directory of all the SFINCS model subfolders was created.
- A FOR loop was utilized to loop over all the subfolders to load the grid information of each SFINCS model.
- Coordinates of the four corners of the grid was defined to make a bounding box.
- A 3333x3333 mesh was created for the grid, defined by the four corners using “meshgrid” and “linspace” functions.
- A mask variable or matrix was defined, with the resolution and size kept consistent with the grid and input information.
- Next, a nested loop function was used to loop through the “polygon.ncst” data in the shapefile.
- The “inpoly2” function (Engwirda, 2023) was utilized to check which points of the created meshgrid falls within the shapefile.
- The output variable from the “inpoly2” function is a logical matrix with ones where the set of vertices are inside the polygon.
- Using this logical matrix, the mask matrix was updated with ones with the indexing kept consistent.

- At this stage a 3333x3333 matrix filled with ones in the active areas deemed by the polygon was the outcome.
- The "inpoly2" function is unable to define the boundary grid cells properly. The process that was implemented within the code was to do 4 sweeps across the grids from all ends.
    - Checked for ones and also whether it is adjacent to a zero by checking the elements above, below, left and right. If both conditions were met, the value of the element was changed from one to two.
- Next step was to define the outflow boundary cells.
    - All the one values at the top, bottom, left and right of the mask matrix were converted to three to complete the mask file.
- Final step was to write the mask files in ASCII format to each of the subfolders that was being looped over.

These ASCII format mask files was written in bin format later with the required depth and manning inputs for the flooding simulations. Given below in Figure 4 is an example of the mask file setup for one particular SFINCS model.

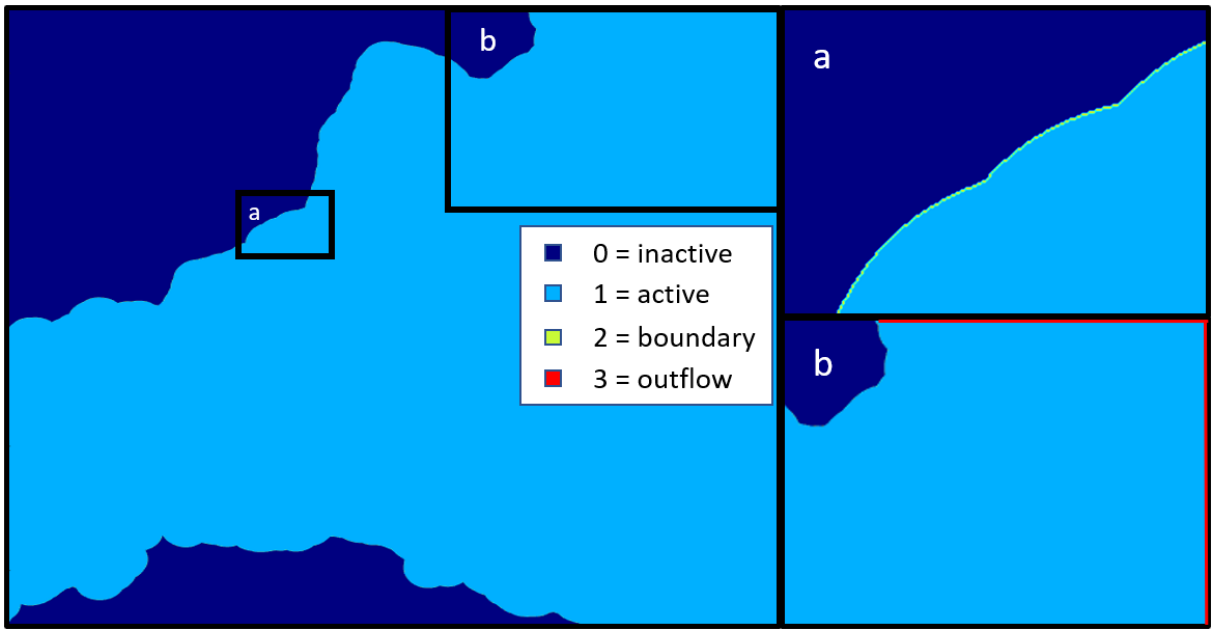

Figure 4: Plot of the overall Mask file (left); (a) Boundary cells with the mask value equal to 2; (b) Outflow boundary cells with the mask value equal to 3

3.4 Supplying the Elevation Data

Elevation data is another mandatory input to the SFINCS models. Elevation data consists of the local topography and the bathymetry data for the model. It is critical for obtaining accurate flood model results and offers information on the terrain's height and slopes, which are significant components in determining how the water will flow during a flood event. DEMs that illustrate the topography of the land surface, including heights of landscapes, roads and other features that can affect the flow of water is used to create the "sfincs.dep" file that defines the elevation or depth for the SFINCS model.

The elevation is defined positive upwards in SFINCS, meaning topography has positive values and bathymetry negative with respect to a particular datum. The reference level is not separately defined in SFINCS input and is not relevant, but the user should keep consistency in defining the levels in other input parameters such as the water-level time-series for the boundary conditions (Deltares, 2022). For this research, Copernicus DEM (COP-DEM) GLO-30, which gives coverage at 30m resolution was utilized (The European Space Agency, 2021). The data was in the form of GeoTIFF files with each tile representing 1 degree in latitude and longitude. Hence a single grid of a particular SFINCS model, could require elevation input from multiple GeoTIFF files to fully define the elevation within that grid. The depth files were also created using MATLAB and the procedure used is given below:

- FOR loop was used to loop over all the subfolders. Within the loop the grid information was loaded and the grid bounding box was defined with the specification of the four corners for all grids.
- A directory of all the reprojected GeoTIFF files and the original GeoTIFF files in the WGS84 projection was made. The check for the GeoTIFF files that overlaps with the grid extents were executed using the reprojected GeoTIFF files as the grids and the SFINCS model are based on the ESPG:3035 projection. However, the reprojected GeoTIFF files are not recommended for the merging and clipping process later as their edges do not align well and produces elevation data gaps between the merged GeoTIFF files. Therefore, the original GeoTIFF files with the same name are required to produce a comprehensive merged TIF file.
- The reprojected GeoTIFF file data was saved in a MATLAB structure using the "geotiff_read" function (Ahn, 2023).
- A nested loop function was created with each bounding box being checked against all of the relevant GeoTIFF files to see if a particular TIF file was required to provide elevation data within that grid extent.
- "inpoly2" and "InterX" functions were utilized to conduct 3 checks:
    - Whether the GeoTIFF file is inside the grid
    - Whether the grid extent is inside the GeoTIFF file
    - Whether the GeoTIFF file and the grids cross each other
- An IF function was utilized and if any of the checks gives a logical output of one:
    - The source folder where the original WGS84 GeoTIFF file is saved was defined.
    - The destination folder, which is the relevant subfolder was defined.
    - The name of the GeoTIFF file to be copied was defined.
    - The full file path of the GeoTIFF file and destination folder was constructed.
    - The GeoTIFF file to the respective subfolder was copied.
- The check is being done with the reprojected GeoTIFF files and original GeoTIFF files of the same name are automatically saved for further processing. This step was executed

for each of the bounding boxes and at the end all the GeoTIFF files that contribute elevation data to the relevant grid is saved in the subsequent SFINCS model subfolder.

- Next from another script, all the SFINCS model subfolders was looped over again and within the FOR loop the following steps were executed:
    - The grid bounding box information was set and xmin, xmax, ymin and ymax (the four corners) were determined.
    - A list of GeoTIFF files as arguments for the "gdalbuildvrt" command was created
    - A virtual mosaic of the GeoTIFF files saved in the subfolders was built using the "gdalbuidvrt" merge command.
    - The merged VRT file was converted to a single band GeoTIFF file using "gdal_translate" command.
    - Before clipping the merged GeoTIFF file to the grid extents, the file was reprojected to project projection, ESPG:3035 using "gdalwarp" command. Also, the "-tr" function was used to set the resolution of the resulting GeoTIFF file to 30m for consistency throughout the inputs.
    - Then the reprojected and merged GeoTIFF file was clipped to the grid bounding box using the "gdalwarp" command and the "-te" function within it, to the grid extents which were defined earlier.
    - To save storage space, the original GeoTIFF files and the merged GeoTIFF files were deleted within the subfolders as only the clipped GeoTIFF file is required to proceed further in creating the depth input file. This was also done within the script.
- At this stage the clipped elevation GeoTIFF file for the relevant grid is saved within the respective SFINCS model subfolder.
- It is optional, but also good practice to verify the elevation from the produced GeoTIFF file by creating an XYZ file using the "data_io_tif2xyz" function (J.Reyns, personal communication, February 04, 2023) and plotting the XYZ file. This is not necessary for the input of the SFINCS model but was done during this study for the models.
- The clipped GeoTIFF file contains the elevation information needed for the "sfincs.dep" file. To read the GeoTIFF file in MATLAB, as before "geotiff_read" function was used.
- The z information of the GeoTIFF file was then stored in a separate variable and the "flipud" function was used to flip the matrix.
    - The GeoTIFF information is saved with mapx and mapy values representing the easting and northing from the file's upper-left corner. However, while the origin point is geographically lower left corner, SFINCS input text file has the x0, y0 at the upper left corner values with an increasing y value going downwards.
    - The flip is necessary to be consistent with the mask, friction inputs and the coordinates of the model grid
- The final matrix generated was 3333x3333 in size and each variable provides the elevation to grid centres in the SFINCS model. This matrix was written in ASCII format using the "writematrix" function and in BIN format using the "sfincs_write_binary_inputs" function. The function requires the elevation data, the mask input data and generates the "sfincs.ind" index file automatically when the function is utilized. The index file is necessary when SFINCS model is being provided with binary input files.

3.5 Defining the Boundary Conditions

To complete the SFINCS input, it is also mandatory to provide some form of information on the model forcing. This could be water-levels, wave information, river discharge and/or precipitation. For this model setup, ESL values were utilized to specify a water-level time-series as input to generate the flooding results required. The time series was specified in the "sfincs.bzs" file and the input locations for these water-levels time-series was specified in the "sfincs.bnd" file. Both of these inputs were specified in ASCII format as the solver manual instructed. This fed the forcing required to run the simulations to the defined boundary cells with a mask number of two as elaborated previously in Section 3.3. A water-level time-series needs to be specified for each boundary point specified to keep it consistent.

Derivation of ESL data was briefly explained in Section 2.2 and for this research the data utilized to generate the boundary conditions was adopted from previously conducted research (Vousdoukas, et al., 2018a). The received ESL data consists of the point location and an extreme water level at each point with the points along the European coastline at approximately 25km. Baseline median data for a return period of 1 in 100 years was utilized for this study. Figure 5 presented below shows the ESL data points represented on the map.

Figure 5: Visualization of the ESL data points

Since the ESL data consists of single extreme values per location, to incorporate a temporal component for the water-level to vary over time, hydrographs were needed to be produced and written into the "sfincs.bzs" file. For this research, similar to Vousdoukas, et al. (2016) synthetic hydrographs were adopted to create the required water-level time-series. A triangular synthetic hydrograph was considered with peak level being the magnitude of the ESL at a particular point and the base width of the triangle was determined by the estimated storm event duration generated from Maximum Meteorological Tide (MMT) levels. The methodology adopted to create the synthetic hydrographs (M. Vousdoukas, personal communication, January 30, 2023) is further elaborated below:

The event duration is given by the equation:

Equation 1

$$Event\ Duration = 8\ \times MMT + 10$$

- To evaluate the event durations, MMT values for Europe were obtained from European Commission's Joint Research Centre (JRC) datasets. Extreme Storm Surge Levels (ESSL) at the European scale were extracted online.
- According to The Joint Research Centre (2015), the ESSL are calculated based on the Peak Over Threshold technique, using an ensemble of 8 meteorological models for the period 1/12/1969 to 30/11/2004 and for 8 return periods (5, 10, 20, 50, 100, 200, 500, 1000).
- From the downloaded netcdf file, the longitudes, latitudes and the ESSL values for all return periods were extracted and saved as a CSV file using MATLAB. The coordinates for the ESL and ESSL points did not align and the datasets had different vector sizes too. So, the next step was to identify the ESSL points that were closest to the ESL points to estimate and assign an event duration to that ESL point.
- "dsearchn" MATLAB function was used and an ESSL value was associated with each of the ESL coordinates. Next step was to create the synthetic hydrographs based on the methodology advised.
- Equation 1 given above was used and the minimum and maximum event durations were limited to 12 and 48 hours respectively. A dt value of 0.5 or 30 mins was adopted and "interp1" function was implemented to create the synthetic hydrographs with the water-levels interpolated between the time 0 to event duration and levels starting from zero and ending at 0, with a peak of the respective ESL value at half duration of the storm event. A visual representation of a synthetic hydrograph produced is presented below in Figure 6.
- Different storm events have different durations based on the relevant ESSL magnitude. To process the data in MATLAB, initially all the hydrographs were made to same size by adding extra zero values. Making the vector sizes consistent allowed the hydrograph series to be concatenated together to a single array with the respective X and Y coordinates.
- Next step was to determine which boundary points and coordinates are relevant to certain grids so that they could be saved as "sfincs.bzs" and "sfincs.bnd" files in the respective SFINCS subfolders.
    - Looped over all the subfolders and loaded the grid bounding box data to define the four corners of the grid.
    - >= and =< functions were used to determine the boundary points that fall within the grid extents xmax, xmin, ymin and ymax.
    - The water-level time-series or the synthetic hydrographs was saved in a separate matrix and rounded off to three decimal places.
    - Next the row index of the first row containing a zero was identified and all the rows below it was deleted. The shortest event duration is opted for all the boundary locations to avoid input of zeros or NaN values in the time-series. Also rows with empty spaces are avoided as it will lead to insufficient data per timestep for the simulation.

    - A row of zeros to the top and bottom of the matrix were added and then the time array for the length of the time-series was created. Time is given in seconds for the SFINCS model and the interval adopted for this study was 30 minutes or 1800 seconds.
- The "sfincs.bzs" was then saved in all the SFINCS subfolders within the FOR loop using the function "sfincs_write_boundary_conditions".
- The length of the time-series was then used to update the input information within the "sfincs.inp" file. The Reference date - "tref", Start date – "tstart", and Stop date – "tstop" were appended to the input text file created from before. The tref and tstart was set to 20230101 000000 for all input files. Then the tstop is set to the last time step of the water-level time-series in "yyyyMMdd HHmmss" format.
    - Start time was written as a string and converted to a datetime object.
    - Then the duration of the hydrograph in seconds was added to the start date and the stop date was then formatted to the required format.
    - The dates and the output parameters dtmaxout and dtout were then written to the "sfincs.inp" file using the "fprintf" function. "dtmaxout" and "dtout" were also set to the last time step of the hydrograph as the maximum water level output for the map was obtained as the results for this study.
- To complete the input files required for the water-level time-series within the SFINCS model, the "sfincs.bnd" file also needed to be generated. The .bnd file consists of the locations from which the boundary conditions would be provided to run the simulations.
- The reprojected coordinates of the ESL data points form the water level boundary points of the model. The coordinates have been reprojected to EPSG:3035 – LAEA Europe with the help of QGIS.
- The relevant X and Y forcing point coordinates of the grid extents were saved within the FOR loop to all subfolders of the SFINCS models in the advised "sfincs.bnd" file format using "sfincs_write_boundary_points" function.

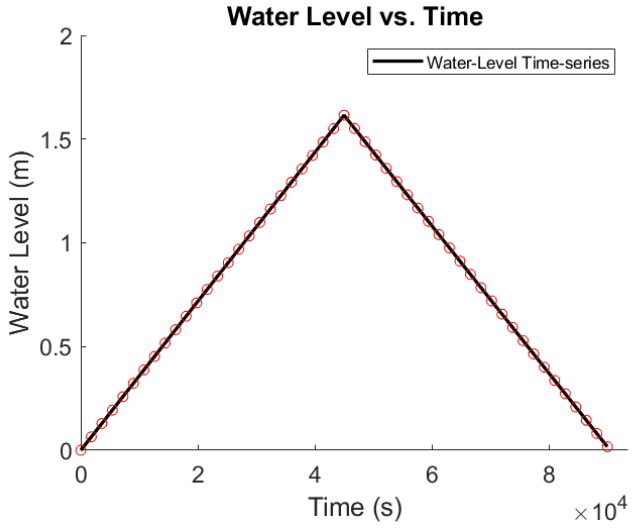

Figure 6: Example of a triangular synthetic hydrograph with the base of the triangle being defined by the duration of the event and the height given by the ESL value at half duration

3.6 Defining the Friction (Manning Roughness Coefficients)

Friction input based on land cover information is optional in SFINCS. However, roughness values can have a significant impact on the flooding simulations as it affects flooding in an area by influencing the speed and volume of the water flow. Surface roughness refers to the amount of resistance that water encounters as it flows across a surface. The rougher the surface, the more resistance there is to water flow, which in turn can cause the water to slow down and potentially accumulate in low-lying areas. For SFINCS models, the user can specify a uniform roughness value, different values for land and sea or can designate a specific roughness value to each grid cell defined.

Friction is specified using Manning roughness coefficient values within the "sfincs.man" binary format input file. A uniform value throughout the grid is highly unrealistic given the different land use variations across the subject areas. Differentiating between the sea and the land was also not considered sufficient. Hence, the adopted methodology to progress was the spatially varying option with specification of a roughness coefficient value to each grid cell. To specify these Manning values, first the land cover type had to be determined. For this purpose, CORINE Land Cover (CLC) data for Pan-Europe was obtained (Copernicus, 2020). The extracted CLC data was a raster, with a format of 100m GeoTIFF file. The CLC 2018 version labelled as v.2020_20u1, covers all 39 European Economic Area (EEA) countries. 44 different land cover types were specified in the CLC file and roughness coefficients had to be assigned to them. Used CLC data is presented below in figure 7.

Average values of Mannings' roughness coefficients were obtained from Papaioannou, et al. (2018), who utilized commonly used roughness coefficient tables (Chow, 1959) to estimate the friction values in their respective study. The relevant roughness values associated with each land cover type is given below in Table 2 for reference. As with other input files, MATLAB was utilized in assigning roughness coefficients to the data points of the land cover GeoTIFF file to produce the "sfincs.man" input.

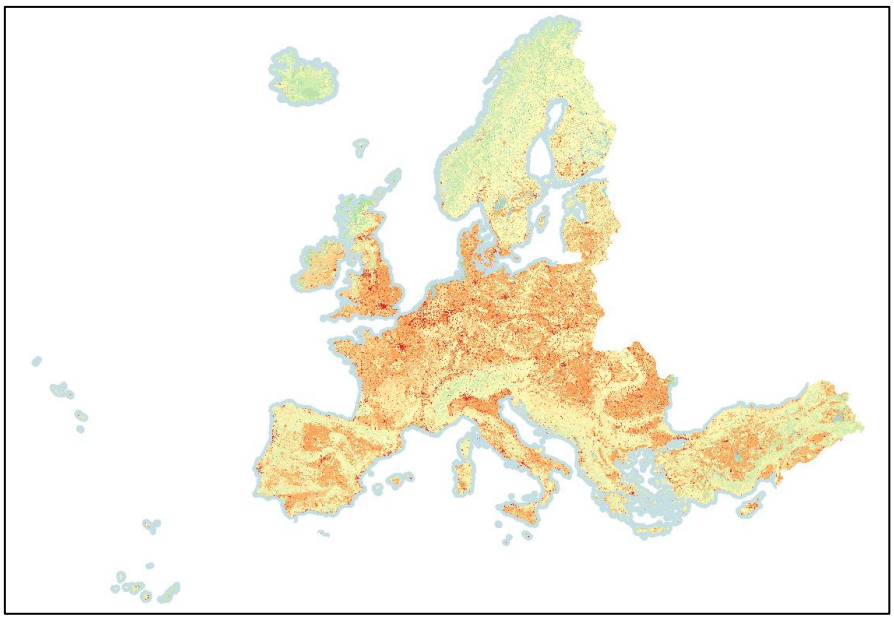

Figure 7: CORINE Land Cover data for Pan-Europe

Table 2: Average values of Manning's roughness coefficient based on CORINE land cover data adopted from Papaioannou et al. (2018)

LC Label 1	LC Label 2	LC Label 3	Mannings n
Artificial surfaces	Urban fabric	Conitnuous urban fabric	0.013
		Disonitnuous urban fabric	
	Industrial, commercial and transport units	Industrial or commercial units	0.013
		Road and rail networks and associated land	
		Port areas	
		Airports	
	Mine, dump and construction sites	Mineral extraction sites	0.013
		Dump sites	
		Construction sites	
	Artificial, non-agricultural vegetated ares	Green urban areas	0.025
		Sport and leisure facilities	
Agricultural Areas	Arable land	Non-irrigated arable land	0.03
		Permanently irrigated land	
		Rice fields	
	Permanent Crops	Vineyards	0.08
		Fruit trees and berry plantations	
		Olive groves	
	Pastures	Pastures	0.035
	Heterogenous agricultural areas	Annual crops associated with permanent crops	0.04
		Complex cultivation patterns	
		Land principally occupied by agriculture	0.05
		Agro-forestry areas	0.06
Forest and semi natural areas	Forests	Broad-leaved forest	0.1
		Coniferous forest	
		Mixed forest	
	Scrub and/or herbaceous vegetation associations	Natural grasslands	0.04
		Moors and heathland	0.05
		Sclerophyllous vegetation	0.05
		Transitional woodland-shrub	0.06
	Open spaces with little or no vegetations	Beaches, dunes, sands	0.025
		Bare rocks	0.035
		Sparsely vegetated areas	0.027
		Burnt areas	0.025
		Glaciers and perpetual snow	0.01
Wetlands	Inland wetlands	Inland marshes	0.04
		Peat bogs	
	Maritime wetlands	Salt marshes	0.04
		Salines	
		Intertidal flats	
Water bodies	Inland waters	Water courses	0.05
		Water bodies	
	Marine waters	Coastal lagoons	0.07
		Estuaries	
		Sea and ocean	

The procedure used in MATLAB to produce this input is given below:

- A directory of all the subfolders for the SFINCS models were made.
- The Copernicus CLC GeoTIFF file was loaded to MATLAB.
- A FOR loop was utilized to load the grid information for each SFINCS model.
- The coordinates of the four corners of the grid was defined to make a bounding box.
- The CLC GeoTIFF file was clipped to the grid bounding box using the gdalwarp command
    - 'gdalwarp -te %f %f %f %f %s %s', xmin, ymin, xmax, ymax, input_file, clipped_file
- The clipped GeoTIFF file with the land cover information related to the relevant grid extent was loaded and the land cover data within the GeoTIFF file was saved to a matrix that can be processed further
- The land cover data was resized using "imresize" function and the nearest neighbour interpolation. The resolution and the size of the variable should be consistent with the amount of grid cells, mask file and the elevation data.
- The data matrix was flipped using 'flipud' function.

    - Similar to the elevation data, the GeoTIFF information was saved with mapx and mapy values representing the easting and northing from the file's upper-left corner
    - The flip was necessary to be consistent with the mask, elevation inputs and the coordinates of the model grid
- A new variable was created and the relevant manning roughness coefficients was assigned to the respective land cover types using "==", the element-wise equality comparison operator.
- An ASCII format text file to each SFINCS model subfolder was written for checking.
- A BIN format input file using the "sfincs_write_binary_inputs" function was also written to each subfolder which is defined in the "sfincs.inp" file.

Every subfolder should have a "sfincs.man" file that gives the friction input for that model at the end of the process that provides spatially varying friction input to the model using this methodology.

3.7 Setting up the Coastal Protection Input

Adding protection related structures is another optional feature within a SFINCS model. These structures can obstruct or redirect the flow of water mimicking flood hazard reduction or mitigation measures within the simulation. There are 2 options for implementing structures in SFINCS that is utilized in this research. That is creating Thin dam and Weir inputs. Thin dams act like walls with infinite height that completely blocks the flow through the grid cells and weirs have limited height. Therefore, the model allows flux over the weirs given the height of the weir is less than the input water-level on either or both sides of it (Deltares, 2022). For both the weir and thin dam inputs, a maximum of 5000 input points is allowed within one file, so there is a limitation that should be acknowledged.

With the supported input, the user can implement multiple polylines within one file. The "sfincs.weir" and "sfincs.thd" files that represent the weir and thin dam protection structures respectively, needs X, Y coordinates for the start, end and intermediate locations for where the user intends to provide coastal protection. Polylines are then snapped onto the model grid based on the protection points that influences the flow of water within those grid cells in the simulation. How this is executed is illustrated in Figure 8 below. For the input of weirs, in addition to the X, Y coordinates, an elevation level (Z) and a Cd coefficient needs to be provided.

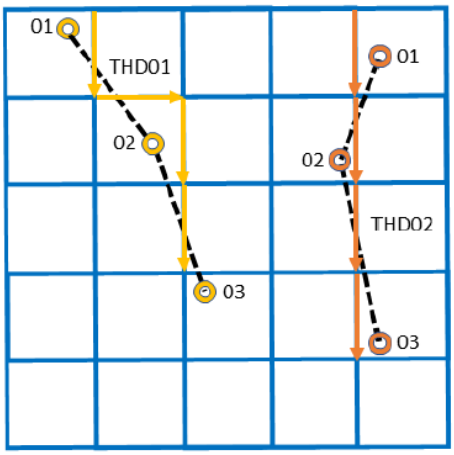

Figure 8: How the weir and thin dam input points are implemented on the model grid and the resulting polylines that are snapped to the grid (SFINCS User Manual Structures, n.d.)

The protection data that would be input to the SFINCS model hence has a significant impact on the output of the simulations. Therefore, providing appropriate protection levels is critical for the quality of the results. The protection data or standards utilized in this study, was generated through a partnership between IHE Delft Institute for Water Education and the JRC. Theoretical protection levels were set based on the return period water levels. These levels are estimations considering population density, urbanization of the region, existence of high value infrastructure such as ports or airports, and economic groups (Bootsma, 2022).

The dataset for protection levels from the collaboration between IHE and JRC consists of a total of 38127 distinct points, with latitude and longitude values plus the relevant return period associated with the protection standards (J. Reyns, personal communication, January 30, 2023). For this study, the relevant protection points for the European coastline was identified and separated using QGIS. The European dataset consists of 6514 protection points with seven protection levels based on 1 in X years return periods with X being: 1,2,10,30,50,1000,10,000. This dataset is presented below in Figure 9.

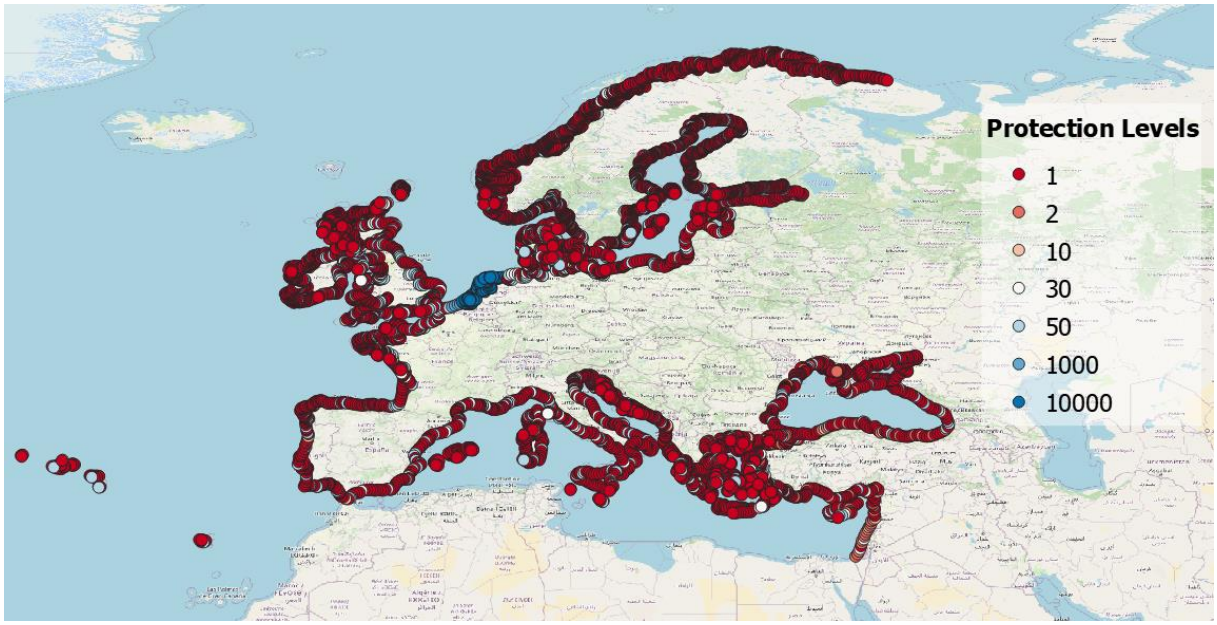

Figure 9: Protection levels for Europe based on the return period.

As with other input files, MATLAB plus QGIS was utilized in assigning protection levels to model with creation of the "sfincs.weir" and "sfincs.thd" ASCII input files. The protection levels were set based on the water level from the respective ESL return period data. However, the ESL data does not cover all the protection level return period specified for the European coastline. ESL data for RP2 and RP30 were not available, hence the height of protection levels for these two cases were separately generated. The steps used in MATLAB to produce this input is given below:

- The protection data text file was loaded to MATLAB and saved as a CSV file to be loaded on to QGIS.
- The protection data points outside of the European region was eliminated in QGIS and reprojected to ESPG:3035 (ETRS89-extended/LAEA Europe) projection, which was adopted for this study. Then the data was extracted as a CSV file with the X, Y coordinates and the protection levels.

- Next step was to generate the ESL data for Return Periods (RP) 1 in 2 years and 1 in 30 years.
    - A polynomial fit is utilized to interpolate between the available return period data (RP1, RP5, RP20, RP50, RP100, RP200).
    - The reprojected data of the available return periods was loaded.
    - A polynomial of degree 6 was fitted to the data using the "polyfit" function with the log value of the return period in years on x-axis and the ESL values on y-axis.
    - The polynomial at log(2) and log(30) was then evaluated using the "polyval" function and matrices were created for the RP2 and RP30 periods for each ESL data point location.
    - The data was then written to CSV files to be further processed.
- All the protection level data was then imported or loaded and the points were classified based on the return period associated with them.
- ESL and the protection points do not align, so similar to ESSL data previously, the ESL data point that is closest to the protection data point was identified and the relevant return period ESL was assigned to that protection point using indexing in MATLAB.
- The X, Y coordinates and the protection level were written and stored in a CSV file.
- The protection points were then plotted with their index number for visualization. For this study the weirs were classified within the script based on the location from the geoplot and according to the coastal country. X, Y, Z and Cd parameters were input for each weir.
- If the protection points were lacking to snap a proper polyline to the coast, additional points were created using QGIS with the protection level assigned based on the closest available protection data point.
- "sfincs_write_obstacle_file_1par(inp.weirfile, weirs)" function was used to create the input file and for more details please refer to the SFINCS manual and MATLAB scripts from this thesis presented in Appendix C.
- In a similar manner, thin dams file was created and copied to all relevant SFINCS model subfolders using MATLAB.
    - Thin dams were associated with Netherlands and Belgium, as only those countries had protection levels of 1 in 1000 and 1 in 10,000 years. Hence, an infinite wall of protection was considered appropriate for the coasts of these countries.
- "sfincs_write_thin_dams (inp.thdfile, thindams)" function was utilized to create the "sfincs.thd" file with the X and Y data for the protection points along the Belgian and Dutch coast.

3.8 Post-processing of the flood data

The output data for the SFINCS models are in Network Common data Form (NetCDF) format. To analyse the results for flooded area (FA) and fit metrics, these NetCDF files needed to be processed first. The methodology plus detailed steps are outlined in the chapters gives below.

3.8.1 Creating GeoTIFF files

The results of the SFINCS simulations, which are in NetCDF format was first converted to GeoTIFF files to make the flooding analysis using QGIS. GeoTIFF files for each of the SFINCS sub-models were created and then merged to form one single GeoTIFF files based on the location. With overlapping due to the multiple grids in use and the complexity plus irregularity of the coastline, the maximum water level for common grid points needed to be determined. The merger results in a common GeoTIFF with maximum water levels for overlapping cells in a single file for better visualization and processing of the results. The initial GeoTIFF files were created using MATLAB and the merging process was done in PYTHON using "gdal" functions. The details of the steps taken are presented below:

- Using the a FOR loop, the results in the SFINCS subfolders were looped over.
- Shapefile of the coastline was utilized to eliminate the results data that were between the buffer outline and the coastline.
- "m_shaperead" as previously mentioned was used to load the shapefiles to MATLAB and "ncread" function was used to read the results data from the NetCDF file.
- A mask was created to eliminate the unnecessary flood levels using the "inpoly2" function. The inputs were the X and Y data from the NetCDF files and the "shapefile.ncst" data.
- Using indexing the mask created was applied to the maximum water level data from the NetCDF files and then the data was converted to centimetres and rounded off to the nearest integer.
- This data was then saved int16 format and flipped before converting to GeoTIFF files as the convention for grid coordinates in GeoTIFF files is the opposite.
- A bounding box was determined using the minimum and maximum values of the X and Y data of the resulting NetCDF file, which should be consistent with the initial grid bounding box for the model.
- This bounding box and the file name were used as input for the "geotiffwrite" function (Shen, 2023) that created GeoTIFF files for results of each grid.

At this stage of the process GeoTIFF files were stored in each subfolder for the respective SFINCS model. Based on the location of the simulation runs, the files were then merged using PYTHON.

- All the relevant results GeoTIFF files were saved in one folder and the directory was input to the script
- From "osgeo" library "gdal" was imported and "gdal.Warp" function was utilized.
- All the GeoTIFF files names were appended and used as input file with an output file specified. The option provided were as below:
- ="-overwrite -multi -wm 80% -t_srs EPSG:4326 -co TILED=YES -co BIGTIFF=YES -co COMPRESS=DEFLATE -co NUM_THREADS=ALL_CPUS -r max -ot Int32")

3.8.2 Calculating the Flood Areas

The GeoTIFF files contain cells that have flooding information and plenty of empty cells. To calculate the area of flooding using QGIS, flooded cells with water level information was distinguished to limit the area calculation for those cells specifically. To achieve this "Raster Calculator" from the QGIS toolbox was utilized. Every cell with a water level or flood depth greater than zero was classified as one and the rest of the cells are given a value of zero. Next using layer properties, a No data value was assigned which in this was zero. The raster layer now contains only the cells that were flooded.

To find the area of the cells the function "Raster layer unique values report" from the processing toolbox was utilized. The algorithm of this function returns the area and number of cells for each unique value in the input raster layer. In this case, the only unique value is the cells previously classified as one. For the model outputs of this study, output cells are already defined in cartesian coordinates as the projection implemented was EPSG:3035. Hence, the function gives the number of cells and the area in square metres. For the comparison data (Tiggeloven, et al., 2020), the coordinate reference system was set to EPSG:4326 where the units are given in degrees latitude and longitude. Therefore, for a direct comparison and analysis the GeoTIFF files were reprojected to EPSG:3035 in QGIS by exporting it in the target coordinate system. Then the same function was applied on this data set and the area per cell in square metres was obtained.

To improve the evaluation of the FA inundation of surface water needed to be neglected. FA in the GeoTIFF files that coincides with water bodies or presence permanent surface water was removed using data from Global Surface Water Explorer (GSWE). Pekel, et al. (2016) from JRC, in conjunction with Google assessed variations in world surface waters and generated maps that show changes in the Earth's surface water. Recurrence data was utilized as it refers to the repeated appearance of water in certain regions and QGIS was used to eliminate these areas from the flood estimates. Intersection of the raster layers were identified and the flood estimate outputs from the models were clipped accordingly.

3.8.3 Fit Metrics to Compare Flooding Results

To assess the results of the simulations of this study by comparing it to Tiggeloven, et al. (2020) flood model results, metrics known as hit ratio, critical success index and false alarm ratio was used. For the calculations, the results from this study was considered as modelled and the other one as observed, assuming that study was more comprehensive and realistic, while the results of this study represents a more theoretical or idealized version of the flooding phenomenon.

The hit ratio was calculated by equation 2 given below to evaluate the similarity in both model results. It determines the flooding extents in terms of cells that are in consensus with each other by evaluating the cells that the SFINCS models flooded, for which the flooding was predicted in the comparison model too. $F_m \cap F_o$ provides the area for which both the models predicted flooding and the denominator is the total observed FA.

Equation 2

$$Hit\ ratio = \frac{F_m \cap F_o}{F_o} \times 100$$

Critical success index given in equation 3 below, determines the area accurately predicted by the results determined as the model versus the union or all of the flood area estimates of both the model results and observed results. If the intersection (numerator) and union (denominator) are similar the success index increases accordingly.

Equation 3

$$Critical\ success\ index = \frac{F_m \cap F_o}{F_m \cup F_o} \times 100$$

The false alarm rate, given in equation 4 below, indicates the flooding extents that SFINCS model estimates, that are missing in the comparison results, hence the given term. This can be considered the opposite of the hit ratio, where the disagreement between the results are quantified. This indicates the potential overestimation by the model results in a comparison study. The numerator defines the flood extent that was only predicted by SFINCS.

Equation 4

$$False\ alarm\ ratio = \frac{F_m - (F_m \cap F_o)}{F_o} \times 100$$

The metrics and their respective equations presented above provides the agreements and disagreements between the compared results. The hit ratio, critical success index and false alarm ratio provides an evaluation of similarly flooded areas, accuracy in overall prediction and the degree of overestimation respectively. The results are presented and discussed in the next chapter.

This study was conducted in three phases:

- Literature Review on hazard estimation, ESLs, flood modelling approaches plus uncertainties associated with it, and details on SFINCS.
- Model Setup: Generating the inputs necessary for the SFINCS model on a large-scale. This includes defining the grids, mask files, elevation data, boundary conditions, spatially varying friction data and protection structures.
- Production and analysis of the results and a comparative analysis with a GIS based inundation model from literature.

The model setup was done using MATLAB and QGIS wherever necessary. Grids were generated by using a semi-automated process with in-built checks and the subsequent "sfincs.inp" files and subfolders were created within the same stage. Land boundary data and buffer zones assigned based on these boundaries were utilized to create the mask files, that assigns a value of one to land, two to the boundary cells, three to the outflow boundary cells and zero for the inactive cells representing offshore regions within the grid. DEMs by Copernicus with a resolution was adopted for the elevation data and was cropped to the extent of the grids. The GeoTIFF files that represented the elevation data provided the information required to generate the "sfincs.dep" input files.

ESL data was utilized to generate boundary conditions in the form of water-level time series and the locations associated with the ESL data was used to assign the water boundary points for the SFINCS models. To account for the temporal evolution of the storm, synthetic hydrographs were created consisting of an isosceles shape, with the ESL forming the peak and the base was estimated from storm durations derived using maximum meteorological tides. CLC data from Copernicus was utilized to estimate the spatially varying friction, with average values of Manning's roughness coefficient values from literature assigned to it. Furthermore, protection structures were implemented in the form of weirs and thin dams using a protection level data set assembled from a collaboration between IHE Delft and JRC.

Flood maps with respect to maximum water levels were generated using SFINCS and a methodology for the comparative analysis with another model results was proposed. The results from SFINCS were obtained in NetCDF format and these were converted to GeoTIFF files and flood estimates in recurring water bodies was removed. Fit metrics hit ratio, critical success index and false alarm ratio were adopted to undertake the comparison and analyse the results.

Chapter 4 Results and Discussion

This chapter presents selected flood extent and flood depth results obtained for the reduced-physics solver derived from the methodology developed and elaborated in the previous chapter, with a comparative analysis to GIS based inundation model results (Tiggeloven, et al., 2020). An overview and analysis of the flood extents for certain European locations and the differences in the obtained water level depths are provided. This is followed by key model setup issues that were encountered and a brief outlook on the computational demand of the SFINCS models. Furthermore, the identified limitations as well as uncertainties of the model are discussed and the potential improvements to the methodology and recommendations for future research are presented at the end of the chapter.

4.1 Flood Extents

4.1.1 Flooded area

A baseline return period of 1 in 100 years was utilized to produce outputs from the SFINCS model and was compared to the GIS based inundation model results based on the same return period and for certain locations that are prone to coastal flooding in Europe. These locations are presented below in Figures 10 and 11.

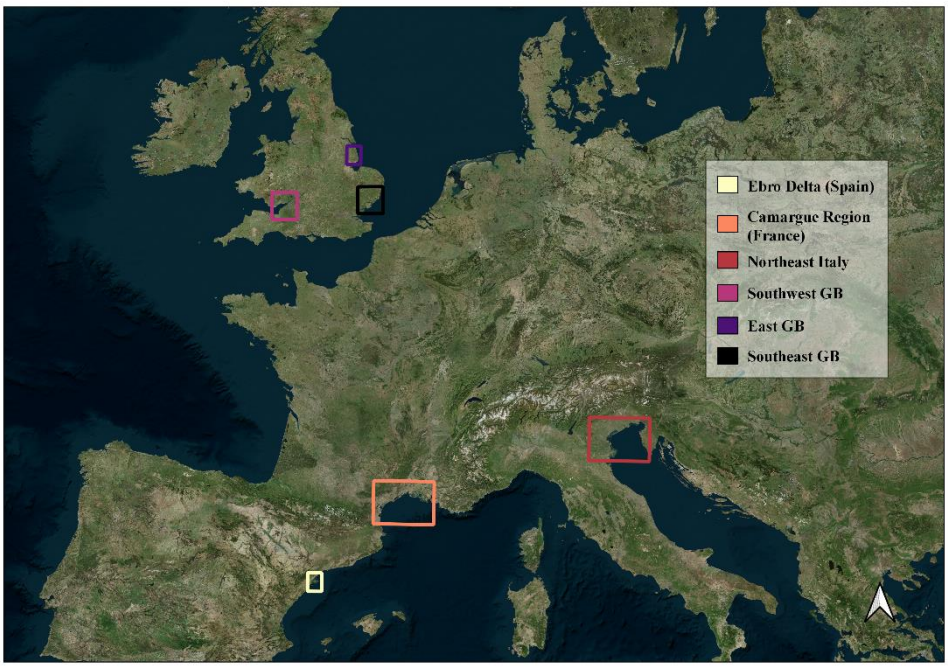

Figure 10: Selected locations for analysis of the results

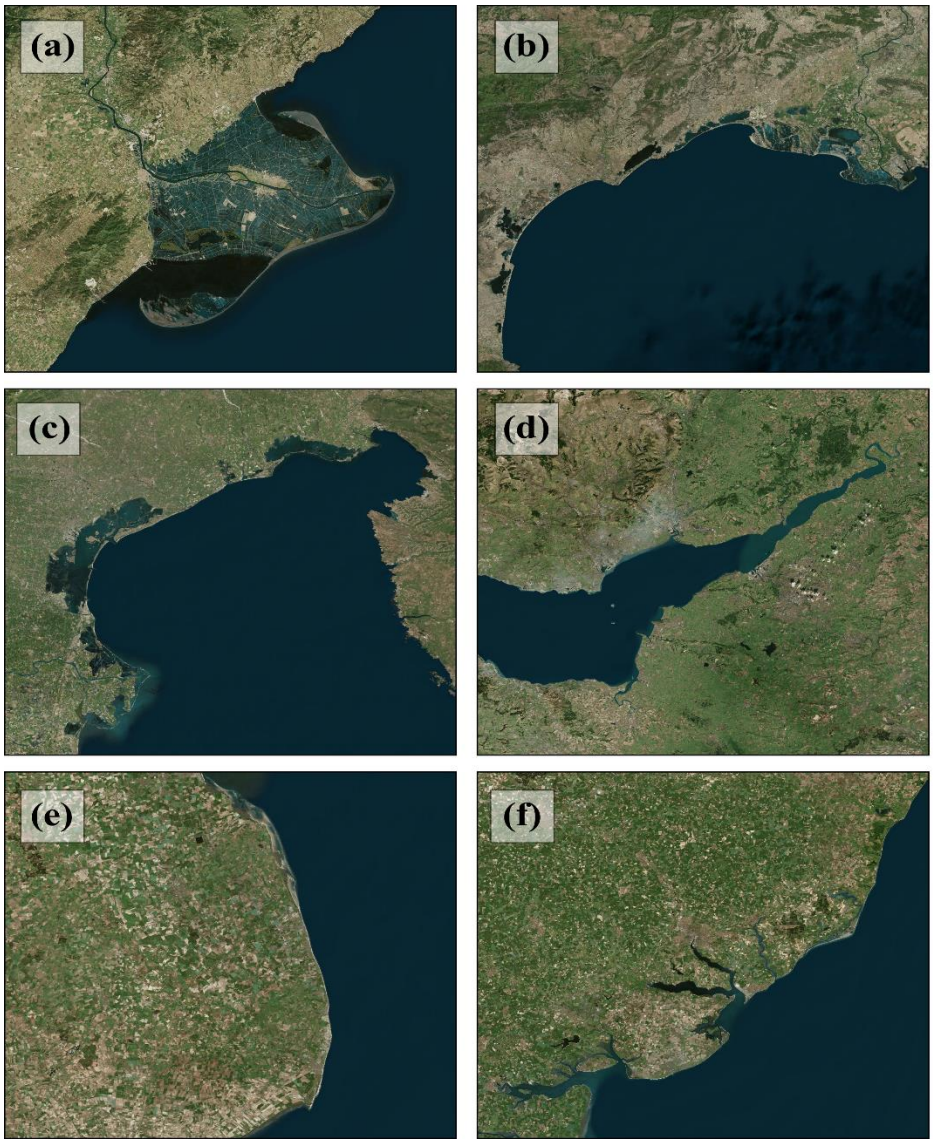

Figure 11: (a)Ebro Delta: (b)Camargue region: (c)Northeast Italy: (d)Great Britain-SW: (e)Great Britain-East: (f)Great Britain-SE

The FA per location in terms of their magnitude and the difference is presented below in Table 3 and Figure 12. The corresponding flood maps are presented in Figures 13 and 14 for visualization of the flood extents in these locations.

Table 3: FA estimated from SFINCS and GIS based inundation models

Location	SFINCS – FA (km^2)	GIS based model – FA (km^2)
Ebro Delta	229.20	189.60
Camargue Region	313.40	164.80
Italy – Northeast	1026.90	1158.60
Great Britain – Southwest	111.50	201.40
Great Britain – East	251.20	206.70
Great Britain – Southeast	194.10	140.70

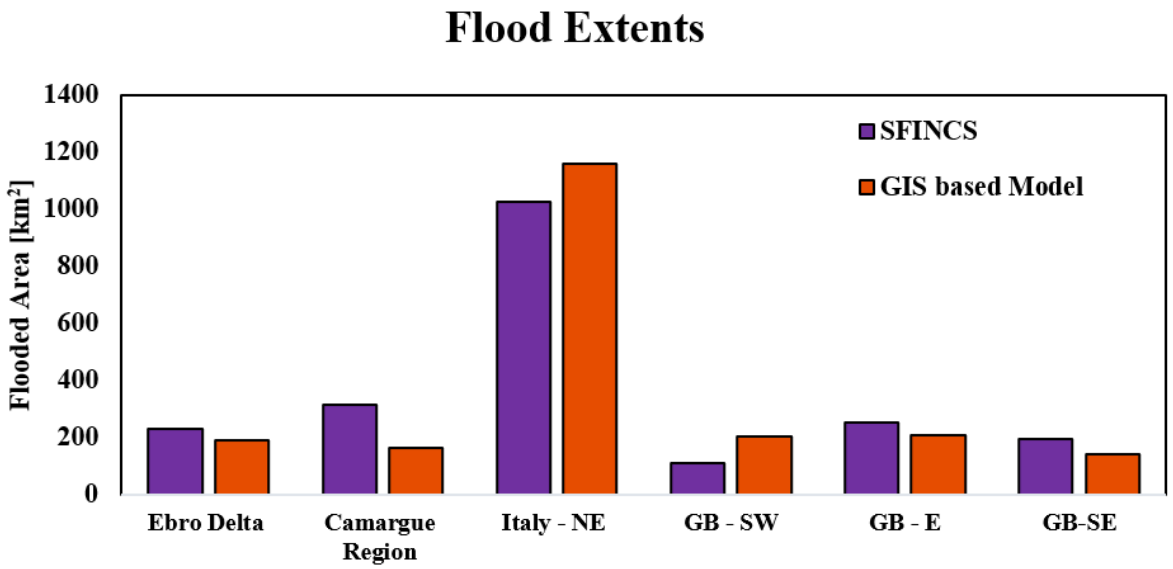

Figure 12: FA estimated from SFINCS and GIS based inundation models

A general trend for the flood extent could not be set based on the results presented above. The SFINCS model predicts a slightly higher FA in the Ebro delta compared to the GIS based inundation model and the difference is not significant. This is not the case for the Camargue region, as the SFINCS model predicts a much higher FA, resulting in a significant difference in the FA. On the other hand, the SFINCS model predicts a lower FA for northeast Italy compared to the GIS based inundation model with a slight difference in the magnitudes.

For Great Britain, the GIS based inundation model predicts a much higher FA for the southwest location with a significant difference between them. However, for both the eastern and southeast locations, the SFINCS model predicts a higher FA with the difference in magnitude being more significant for the southeast location.

From Figure 12 above and Figures 13 plus 14 presented below, it can be observed that the two models' predictions with regards to flood extent and depth differ significantly for some locations, while for others, the difference is not as significant. The SFINCS model predicts a higher FA in four out of six locations compared to the GIS-based model. The differences in the models' predictions could be due to differences in the underlying data such as the DEM data and boundary conditions, assumptions, or modelling techniques implemented.

The DEM resolution implemented in both models differs vastly. As mentioned in Section 3.4, the SFINCS model utilized the COP-DEM with a resolution of 30m. On the other hand, the GIS based inundation model used the Multi-Error-Removed Improved-Terrain (MERIT) DEM (Yamazaki, et al., 2017) at a 30 second by 30 second resolution, which translates to approximately 900m by 900m at the equator. Performance of a flood model can vary significantly depending on the resolution utilized. A model with a finer resolution would generally tend to produce more accurate results as it allows for more detailed representation of the terrain which could result in a more accurate simulation of the water flow. Nonetheless, SFINCS models developed based on the methodology were capable of predicting flood-prone regions and flood estimates when compared to the GIS based inundation model.

As for the boundary conditions, both models use ESLs derived from global reanalysis data including the addition of tropical cyclones. For the GIS based inundation model wind-waves are not included and the tide is simulated using Finite Element Solution 2012 model (Tiggeloven, et al., 2020). For the ESL values used in the SFINCS model, Finite Element Solution 2014 was used for simulation of the tides and reanalysis data of wind-waves were included (Vousdoukas, et al., 2018a). Furthermore, Vousdoukas, et al. (2018a) generated the ESLs by combining PDFs through MC simulations. This can be deemed a more robust approach that can provide a more nuanced and informative picture of the potential impacts of ESLs. This sort of probabilistic approach was not followed for the GIS based inundation model and could again be a key reason for differences in the results.

Difference in the implementation of the flood protection levels and water propagation techniques in both models can also lead to variations in the results. For the GIS based inundation model, flood protection levels are estimated based on the FLOPROS modelling approach (Tiggeloven, et al., 2020). For the SFINCS models the flood protection data is as outlined in Section 3.7. In terms of flood generation and propagation, SFINCS model has water-level time-series as boundary conditions with temporal evolution and spatially varying friction values which affect the model results. These inputs simulate the behaviour of the floodwaters as they propagate through the domain and provide a realistic representation of how the floodwaters may impact the surrounding areas. For the GIS based inundation model, as highlighted in Section 2.5, a resistance factor was utilized to limit the inland flow and represent the finite time frame of tides and storm surges.

All in all, these differences in input and modelling techniques could lead to the difference in the outputs for the models and would be referred to further in the upcoming comparisons given below.

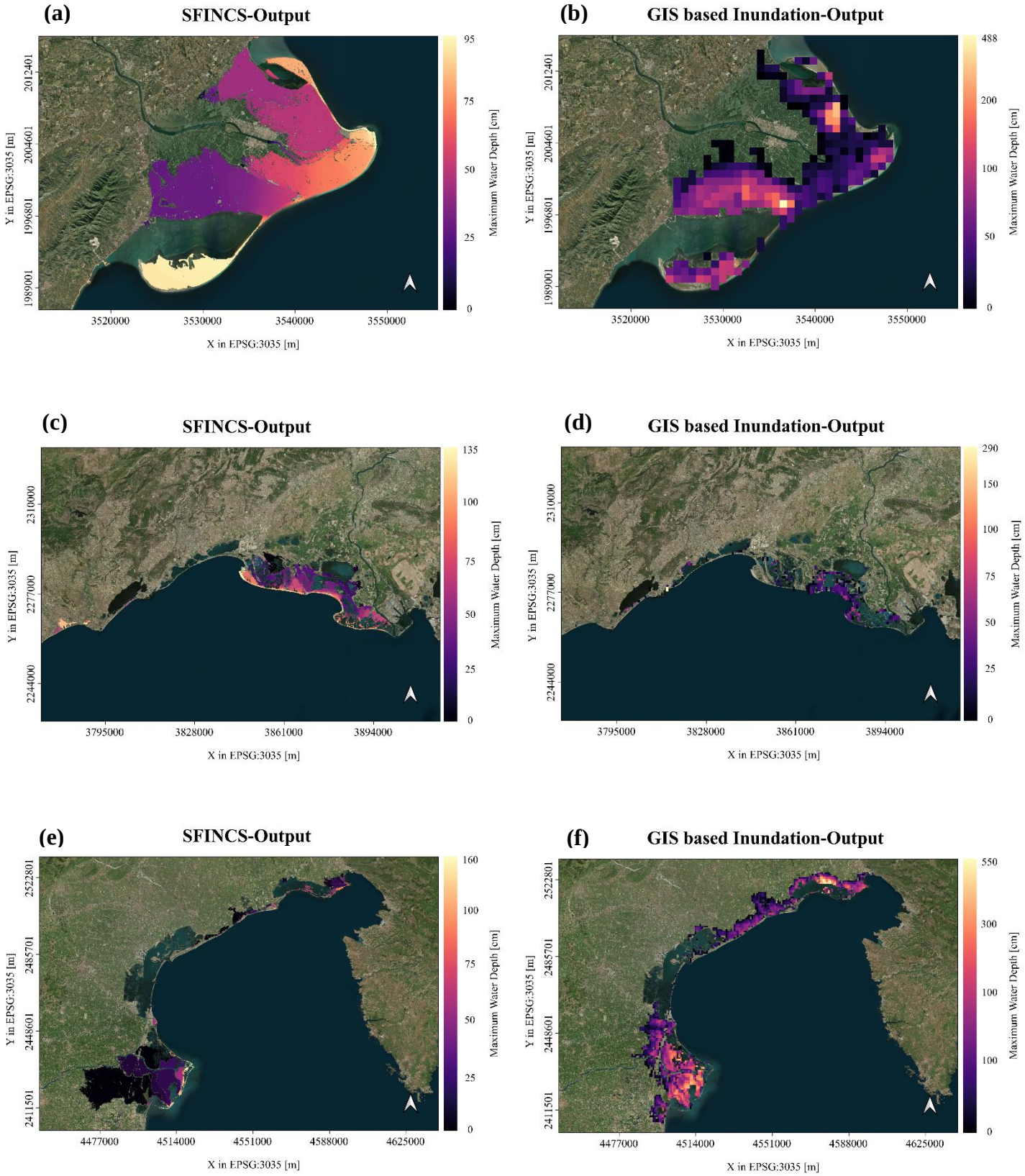

Figure 13: (a)Flood and maximum water depths in Ebro Delta by SFINCS: (b)Flood and maximum water depths in Ebro Delta by GIS model: (c) Flood and maximum water depths in Camargue region by SFINCS: (d)Flood and maximum water depths in Camargue region by GIS model: (e)Flood and maximum water depths in Northeast Italy by SFINCS: (f)Flood and maximum water depths in Northeast Italy by GIS model

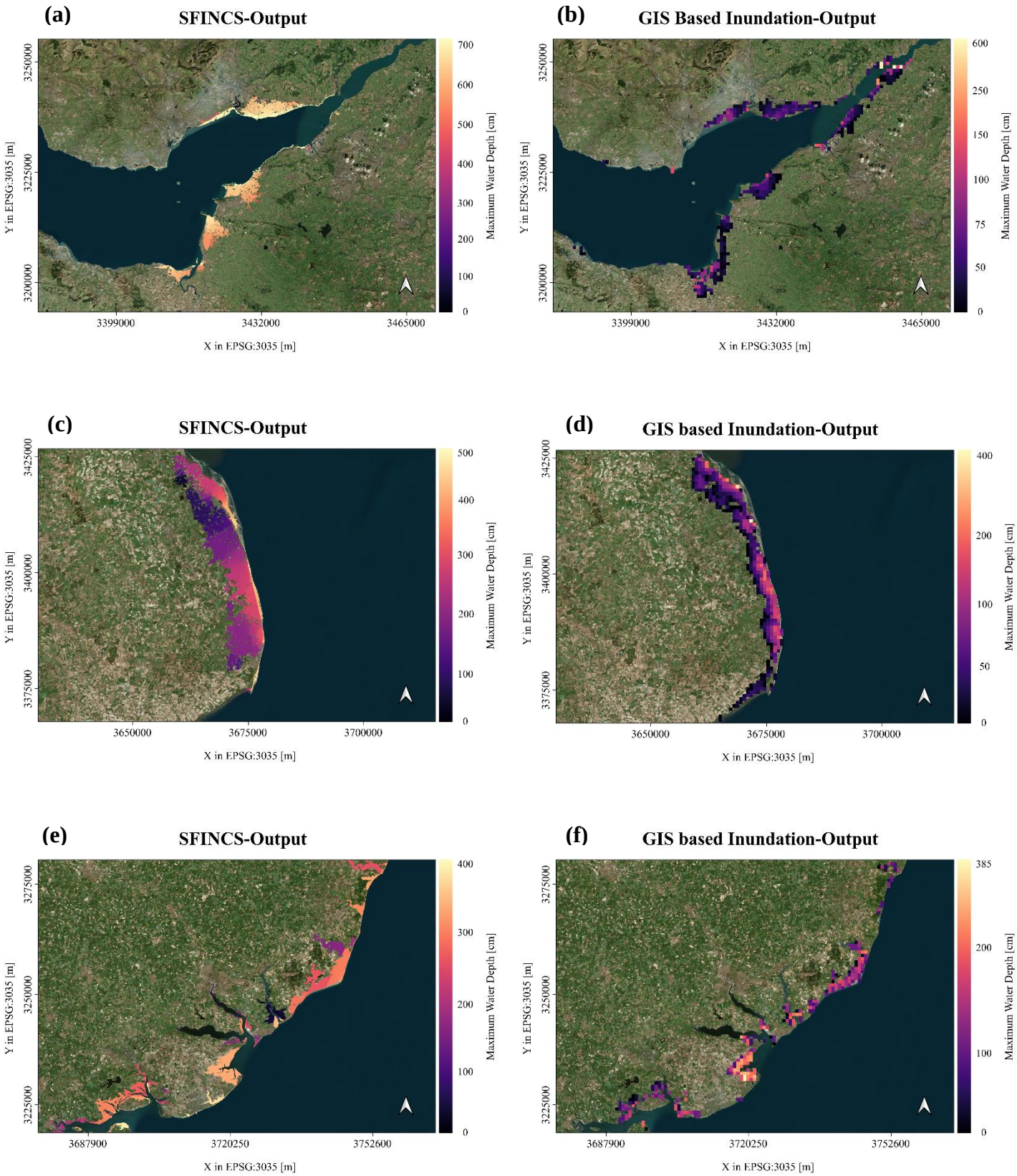

Figure 14: (a)Flood and maximum water depths in Great Britain-SW by SFINCS: (b)Flood and maximum water depths in Great Britain-SW by GIS model: (c) Flood and maximum water depths in Great Britain-East by SFINCS: (d)Flood and maximum water depths in Great Britain-East by GIS model: (e)Flood and maximum water depths in Great Britain-SE by SFINCS: (f)Flood and maximum water depths in Great Britain-SE by GIS model

4.1.2 Fit Metrics

The results of the fit metrics analysis, previously discussed in Section 3.8.3 is presented in this section. The metrics were calculated specifically for the locations mentioned above and include the hit ratio, critical success index, and false alarm ratio. A summary of the computed values is presented below in Table 4 and Figure 15. Equations 2, 3 and 4 presented in Section 3.8.3 were used to calculate the hit rates, critical success index, and false alarm ratio respectively.

Table 4: Fit metrics calculated for specific locations

Location	Hit Ratio (%)	Critical Success Index (%)	False Alarm Ratio (%)
Ebro Delta	86.62	65.66	34.28
Camargue Region	54.80	23.50	135.40
Italy – Northeast	41.80	28.50	46.80
Great Britain – Southwest	35.92	29.74	19.41
Great Britain – East	70.87	41.17	67.11
Great Britain – Southeast	69.10	43.21	52.40

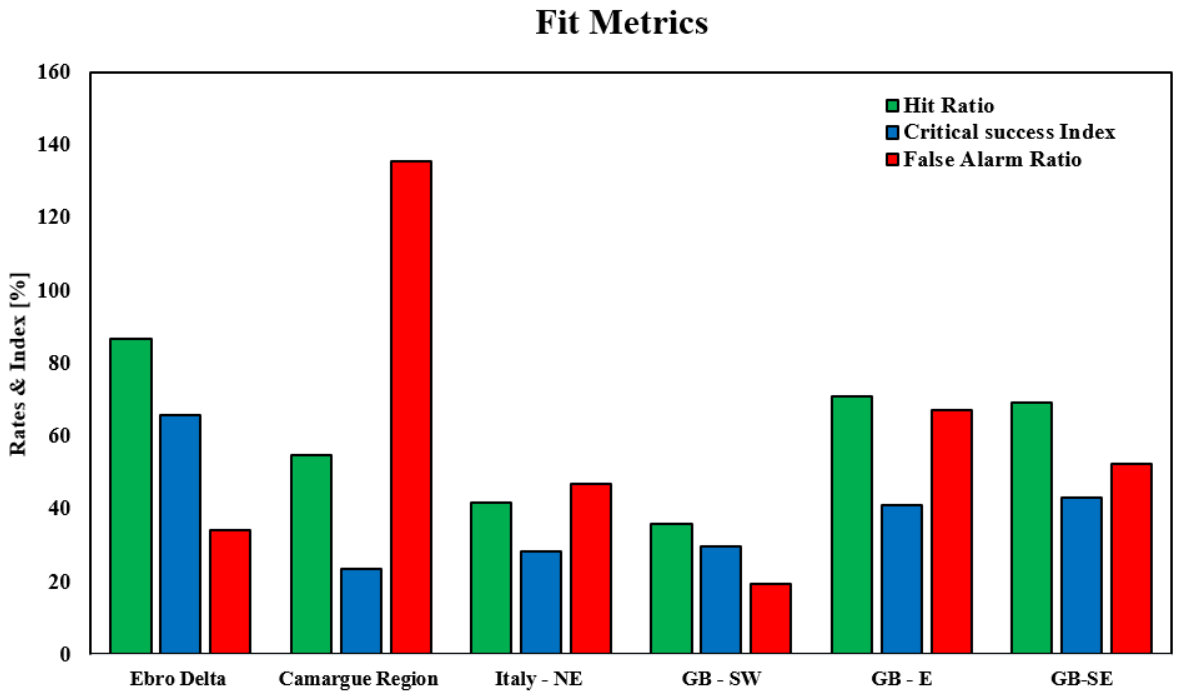

Figure 15: Calculated fit metrics for specific locations

The hit rates obtained show that for the majority of the locations, SFINCS and the GIS based inundation model results are in good agreement with each other. For two locations, the Ebro delta and the Camargue region, the hit rate is significantly high meaning SFINCS models predicted a large amount of area for which flooding was also predicted by the GIS based

inundation model. For the locations, east Great Britain and southeast Great Britain, both models are in good agreement with each other in terms of the hit rate but is not as high as the locations mentioned previously. However, the performance of the SFINCS model can still be considered good in comparison, as SFINCS generally predicts flooding in areas the GIS based inundation model estimated too.

For both northeast Italy and southwest Great Britain, the SFINCS model agrees with a smaller portion of the FA estimated by the GIS based inundation model. With a hit rate below 50% for both locations, it can be deduced that SFINCS has underestimated the flood extent in comparison. This can be due to the flooding techniques implemented in terms of propagation and protection levels specified in the input. The GIS based inundation model predicted a higher rate of inundation at the mouth of the River Severn estuary in western Great Britain and the Po delta plus area adjacent to Venice lagoon in northeast Italy. With a higher model resolution, spatially varying friction values, and location specific protection levels, the results of the SFINCS model could be deemed more accurate and a better representation of a flooding event for 1 in 100-year return period.

The results for the critical success index are consistently less than the hit ratio for all locations and is above 50% for only Ebro Delta. For all other locations analysed, the metric ranges from approximately 30% to 43%. This indicates a poor degree of agreement between the model results and a noticeable lack of consensus between the predicted FA. With the difference in dynamic inundation techniques compared to the GIS based inundation modelling (bathtub approach), these results are expected as the dynamic methodology of SFINCS would not fully agree with the aforementioned method. However, with the use of resistance factors to emulate water-level attenuation, the GIS based inundation model does appear to have limited the overestimation of flooded areas that is expected of such models.

The false alarm ratios calculated can be deemed consistently low apart from the ratio for the Camargue region. This indicates that the SFINCS model does not overestimate the FA in comparison to the predictions from the GIS based inundation model. This can be deemed a positive result as the GIS based planar inundation models tend to significantly overestimate flood extents as per discussion in Chapter 2. This was not the case, particularly for the Camargue region in these results. However, the region has a considerable amount of low elevation areas and water bodies. With the higher resolution, the SFINCS model probably was able to more accurately predict the flooding in this region with greater details of the terrain at disposal. This could be the reason for the higher false alarm hits in this instance, which can be deemed a valid outcome from the SFINCS model. The next highest false alarm ratio was obtained for the eastern location of Great Britain. The SFINCS model predicts a larger flood extent inland from the coast as seen in Figures 14(c) and 14(d). This could potentially be an underestimation from the GIS based inundation model due to the implementation of resistance factors to limit the flood propagation, resulting in a higher false alarm ratio when compared to the SFINCS model.

Overall, a significant agreement between the model results was not obtained across the board based on the locations analysed and the computed fit metrics. It can be established that the SFINCS models developed based on the methodology presented is sufficiently capable of estimating flood extents on a large-scale. Significantly high hit rates were obtained and the false alarm ratios were low for majority of the locations. In general, the implemented SFINCS model results can be deemed acceptable accounting for the uncertainties plus variation in the compared models with regards to the elevation accuracy and resolution, boundary conditions (ESL values), attenuation techniques, and implementation of flood protection standards or structures.

4.2 Flood Depths

Apart from the FA and flood propagation extents, the performance of the SFINCS models is also evaluated based on the water levels or the flood depths obtained. For the majority of the locations, a significant agreement in maximum water level results can be seen as presented in Figure 16 below. For northeast Italy, the GIS based inundation model has consistently higher inundation water levels and for western Great Britain, the maximum water levels obtained from the SFINCS model were significantly higher. This could be due to the differences in ESL boundary conditions applied and the flood protection levels implemented. The variation in the maximum water levels obtained was analysed by subtracting the magnitude of water levels of the GIS based inundation model from the results of the SFINCS model and evaluating the extent of areas for a range of differences in the water levels. Hence, negative results indicate a higher water level estimate by the SFINCS model.

For the Ebro delta, the output consists of negative values for approximately 22% of the common FA between the models. The highest difference obtained in water levels for these results was approximately 0.5m. Positive values indicating a higher water level prediction for the GIS based inundation model cover the majority of the study area at 78%. 37% of the common flood extents has a water level difference greater than 1m and approximately 12% has a difference greater than 2m. The proportion of areas for which water level differences obtained are greater than 3m and 4m are 2.8% and 0.4% respectively. The GIS based inundation model results had certain areas with significantly high flood levels resulting in these difference magnitudes.

The Camargue region has a more balanced outcome with regard to the maximum water levels. Approximately 47% of the common FA gave negative results for higher predicted levels from the SFINCS model and the remaining 53% were positive. Around 10% of this area has a difference of greater than -0.5m. Approximately 23% and 7% of the area have differences greater than 0.5m and 1m respectively indicating higher estimates for the GIS based inundation model. For northeast Italy, the results obtained are consistently positive with greater water levels for the GIS based inundation model. Only around 3% of the common FA has negative magnitudes and the difference in maximum water levels are greater than 0.5 and 1m for 80% and 39% of the FA respectively. A very small, 0.3% of the FA gives a difference greater than 5m, but this could be considered a potential anomaly.

For the locations within Great Britain, a general trend can be seen. For all the locations the SFINCS model gives higher maximum water levels for the majority of the FA within the flooding outputs. Approximately 98% of the common FA in the southwest location gives negative values with a difference greater than 1m for the respective extents. The difference in levels is greater than 3m and 5m for approximately 95% and 50% of the areas respectively. The results for the east Great Britain location give higher water levels for the SFINCS model in 96% of the common FA, with approximately 70%, 24%, and 2% associated with differences greater than 1m, 2m, and 3m respectively. A similar outcome was observed for the southeast Great Britain location. 87% of the common FA produced a negative value for higher maximum water levels derived from the SFINCS model. Approximately 48% and 13% have a difference greater than 1m and 2m respectively. Nearly 5% and 2% have water level differences greater than 1m and 2m for areas with positive results, indicating higher levels from the GIS based inundation model.

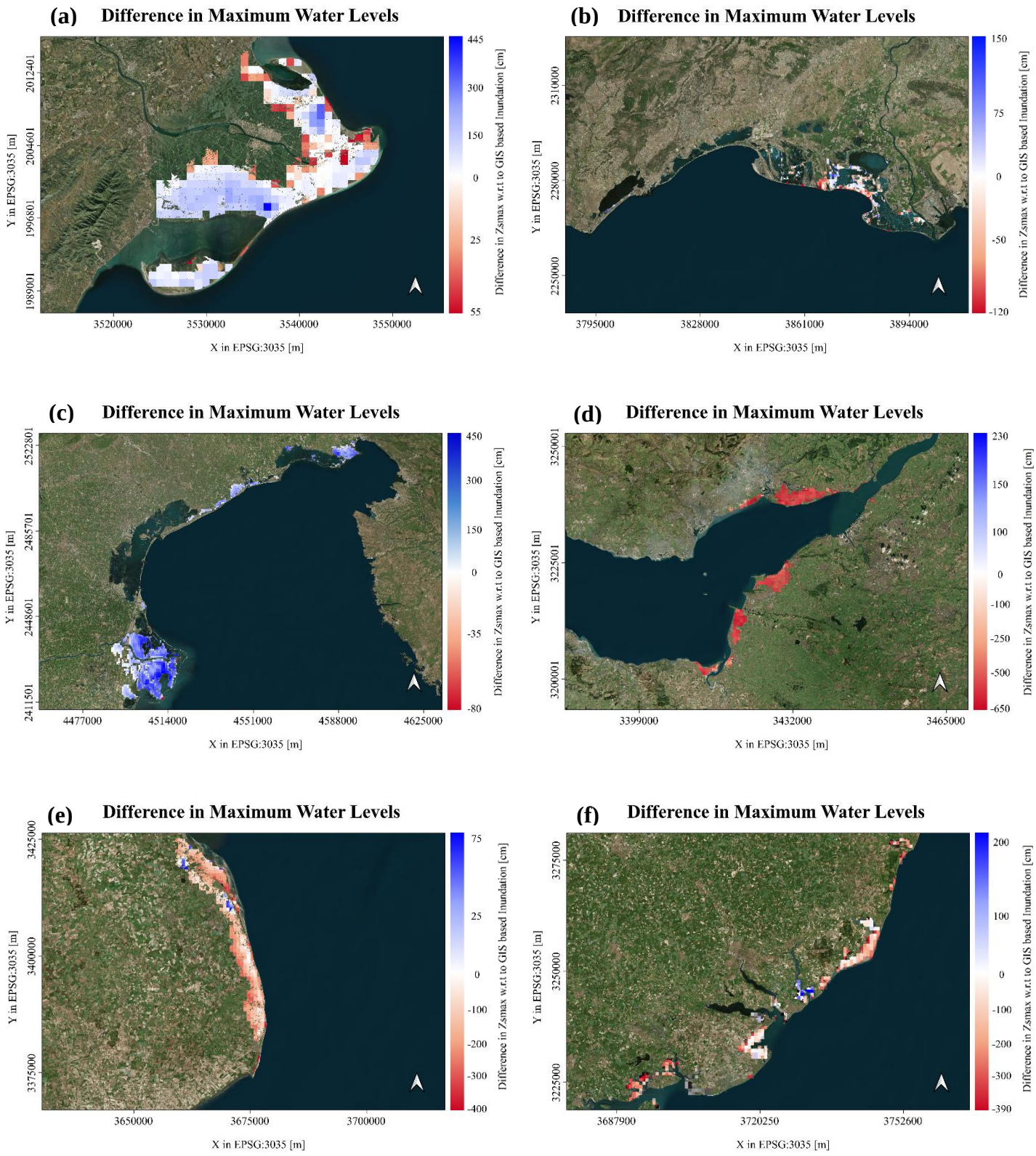

Figure 16: (a)Difference in maximum water levels between the models for Ebro Delta: (b) Difference in maximum water levels between the models for Camargue region: (c) Difference in maximum water levels between the models for Northeast Italy: (d) Difference in maximum water levels between the models for in Great Britain-SW: (e) Difference in maximum water levels between the models for Great Britain-East: (f) Difference in maximum water levels between the models for Great Britain-SE

Figure 16 above presents a visualization of the discussed differences in maximum water levels in this section. These results can be associated with potential variations in the input water and protection levels. Furthermore, the water attenuation technique implemented in the GIS based inundation model can greatly influence the water levels as the flood propagates. The maximum water levels obtained from the SFINCS models are consistent with the ESL values associated with the regions and the flood protection data utilized. Based on the available data and analysis, it can be concluded that the results for SFINCS flood depths are within an expected range and can be deemed acceptable. There is no evidence to suggest that the results should be discarded or rejected based on erroneous or unrealistic outputs.

4.3 SFINCS Model Issues Encountered

During the initial simulations for the SFINCS models, two main issues were identified that resulted in outputs that needed to be discarded. These issues are highlighted for future reference and how it was addressed and resolved is outlined in this section. These issues are related to the input boundary water levels and how the flood protection structures are implemented in the SFINCS model. Figure 17 below shows outputs from western Great Britain that are related to the boundary forcing issue. This issue was identified in other locations too.

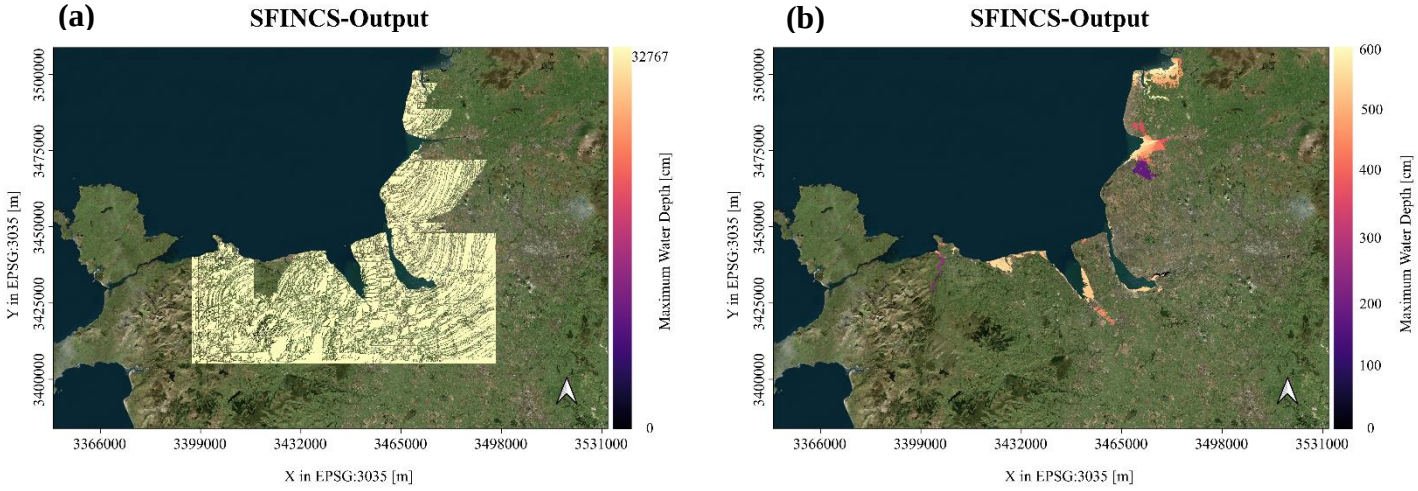

Figure 17: (a) Great Britain–West SFINCS model output with errors or NaN values: (b) Debugged output for the Great Britain–West output

The initial output gave erroneous values as the maximum water levels, which appeared to be NaN values as the water-level time-series forcing was not properly implemented. The propagation of the flooding event from the coastline to inland is also not modelled in this case. The first check in the debugging process was to see if the resolution for input files was consistent. The depth, mask, and spatially varying friction input were verified again before progressing. The first debugging run was done with spatially uniform roughness values. The idea was to make the model as simple as possible and include complexities as the debugging process progressed. This step did not fix the output, so the next measure was to modify the boundary conditions. The water-level time-series were input into the model from particular locations identified in the "sfincs.bnd" file. The process adopted was to start with a low number of boundary input locations and add more in the follow-up simulations.

The reason for the erroneous output was identified to be boundary input locations not being based offshore or inland, and within the masked region. The ESL boundary inputs adopted for the study had default boundary locations that lie within the land area and these points needed to be moved offshore. The boundary input locations were moved to an extent away from the shoreline defined by a buffer layer. After fixing the boundary input location issue, the output from the model was as expected which can be seen in Figure 17(b).

The other issue that was encountered, which did not give ideal results was how the flood protection structures were implemented in the model. As highlighted in Section 3.7, based on the protection input points, polylines are snapped onto the grid of the SFINCS model. However, due to the complex nature and irregular shape of some coastlines, these polylines could be snapped through the land area rather than along the shoreline if sufficient input weir or thin dam points are not supplied to the model. The output from such a case is presented below in Figure 18. To resolve the issue, more flood protection points that were created based on the protection level from the nearest neighbour and using QGIS, were written to the "sfincs.weir" input file, ensuring that the vast majority of the polylines were snapped outside of the land area and not through it. The user also has to be careful not to set the protection structure inputs further offshore rendering them ineffective in terms of the boundary input locations.

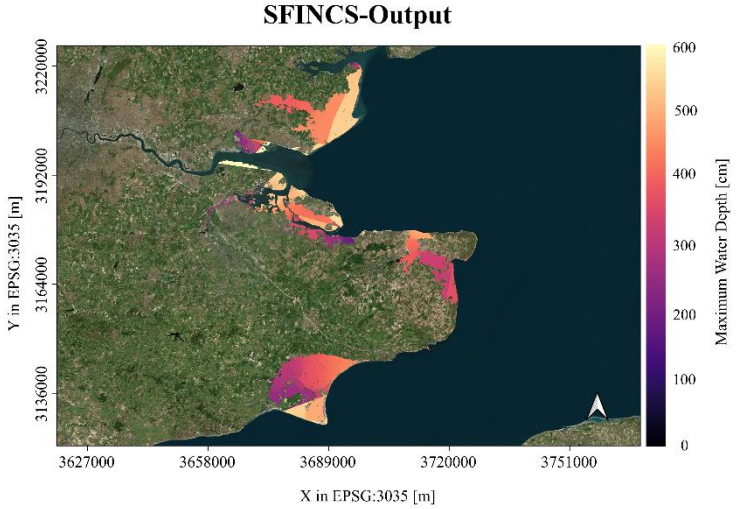

Figure 18: SFINCS output for Great Britain-South with insufficient protection input

It can be seen in Figure 18 above, that there are numerous sharp changes in the water depths within the flood propagation extent. These locations are where the protection structure polyline has been snapped onto the grid of the model. These results are not desirable as they could overestimate the flooding extent due to lack of protection at the coastline itself. They could also result in coastal flooding in areas that are fully protected and flooding should not be predicted in the model.

4.4 Computational Demand

Computational demand and efficiency are critical aspects of flood modelling, particularly on larger scales. As highlighted before, the planar inundation modelling techniques or bathtub models are utilized for large-scale models as the computing time and demand is low. This makes the model type more appealing to undertake large-scale studies and easier to manage for the researcher. Dynamic inundation modelling techniques such as SFINCS have been acknowledged as a potential improvement in studies of coastal flooding with the drawback of increased computational demand and lower efficiency. However, if the demand and additional time needed are manageable, opting for reduced-physics solvers such as SFINCS would be the more proper approach for future studies.

For this study, the simulations were run on two computer systems. Their specifications and performance vary noticeably and the product details are presented below in Table 5.

Table 5: Comparison of the specifications for the two systems used for the SFINCS simulations

Computer System	**IHE User Laptop - System 1**	**IHE High Performance Computer (HPC) – System 2**
Processor (Clock Speed)	Intel i5-8250U 4 Cores (1.60 – 1.80 GHz)	Intel Xeon 8 cores (3.20 – 3.20 GHz)
Random Access Memory (RAM)	8GB (2400 Mhz)	16GB
Storage Type	SSD – NVMe	-
Operating System (OS)	Windows	Windows

Simulations were conducted simultaneously on both the systems for the study and the simulation times were recorded with reference to the generated "sfincs_log.txt" file after each run. Over 250 simulations were conducted for this study and in general, the simulation times presented similar trends. As expected, the performance of System 2 (HPC system) is considerably better compared to System 1. A total simulation time ranging from 20 minutes to 45 minutes was recorded for System 2 with an average total simulation time of approximately 30 minutes. For a grid size of 100km x 100km and a resolution of 30m, this could be deemed an efficient outcome. For system 1, a total simulation time ranging from 75 minutes to 115 minutes was obtained. On average the simulation times were more than double the duration of time when compared to System 2. 65% to 73% of the total simulation time was recorded as being spent in momentum computations and 25% to 33% in continuity computations.

The output NetCDF file consisting of the maximum water level data for each simulation is 508 megabytes. The subsequent GeoTIFF file created from MATLAB is 42.5 megabytes in size. However, the merged and compressed GeoTIFF files from PYTHON were smaller than 1 megabyte, which is more acceptable in terms of storage. For the NetCDF files, a larger size external storage device is advised to reduce the impact on the system storage. Overall, accounting for this demand, for a large-scale study requiring a vast number of simulations, HPC systems similar to the one used in this study are strongly suggested. System 1 or comparable systems with such specifications are not recommended considering the resolution and grid size.

4.5 Limitations of the Models

Limitations of the study are presented both based on the uncertainties within the modelling phase and the post-processing stage of the model outputs. First, the limitations of the GIS based inundation model is highlighted below. Tiggeloven, et al. (2020) identified the main limitations in the model with regard to estimating the flood hazard as follows:

- Lack of dynamic inundation modelling in the model technique
- The low resolution of 30" x 30" being utilized for the modelling scheme
- Estimation of flood protection levels based on the FLOPROS modelling approach which provides an approximate estimate of the present flood protection levels

Using the SFINCS solver with a high resolution of 30m addresses the limitation of the GIS based inundation model mentioned above. SFINCS provides a viable option for dynamic inundation modelling and an efficient solution with regard to computational demand for high resolutions which has been tested during this study. However, even considering the high resolution used in this study, the model potentially could miss details to accurately capture small-scale features such as narrow channels, streams or small-scale terrain variations. Also, the input required for such a model would need to be of a similar level of detail. Otherwise, interpolation techniques are required, such as for the spatially varying friction input in this study. Lower resolution data can again limit the accuracy of the model. Furthermore, based on the availability, the computational resources, including storage space and processing power could potentially be a limitation in conducting a similar study.

Flood protection levels for this study can also be considered as a limitation. The protection standards are estimates determined from the population, infrastructure, and economic state of the regions and might not be a true representation of the current protection standards. With the protection levels being defined by respective return period water levels, uncertainties in those levels are also incorporated to the flood protection structures. Furthermore, the interpolation done during this study for absent data of certain return periods is a gross estimation and a major assumption that was adopted. In addition to this, due to implementation of flood protection structures only on the coastal region, together with the adopted resolution of the DEM, protection structures within the hinterland that could hinder the progress of the flood propagation might be excluded from the model.

Accounting for the temporal evolution of the flooding event within the boundary conditions is an improvement to the static ESL methodology utilized in the bathtub approach. However, this methodology itself has uncertainties. The shape of the synthetic hydrograph representing an isosceles triangle based on the linear interpolation does not accurately represent a storm event. The symmetry on both sides of the peak and the estimation of the storm duration based on the meteorological tide incorporates inaccuracies in the water-level time-series that is being used as input. This methodology is also missing details of variations in the water levels due to time-varying surge and tide components.

The results presented in the study also have uncertainties with regard to the computations done. For both the model output data, GWSE data was utilized to eliminate surface water areas to compare the models and conduct an evaluation of the results. Accuracy of the GWSE database, the influence of currently existing new surface waters, and the inclusion of potential flooding along the shorelines with no infrastructure, induces uncertainties for the FA calculated, which is another limitation of the study.

4.6 Improvements to the SFINCS Model and Recommendations for Future Research

Based on the limitations of this study, improvements can be made to the current methodology in the setup of the SFINCS model. The resolution can be deemed sufficient for large-scale modelling and the subsequent computational demand and efficiency with regard to SFINCS is also manageable. This efficiency can be further increased with the use of SFINCS subgrid approach. The simulation times can be reduced with the use of a coarser grid while still maintaining the accuracy of results as for the regular mode.

Another major area of improvement is the boundary conditions, particularly the water-level time-series. A synthetic hydrograph was implemented in this study, which can be replaced with more realistic storm tide hydrographs. Dullaart, et al. (2022) recently developed a method to create hydrographs referred to as HGRAPHER. This method supplies a global dataset of storm tide hydrographs for 23,266 output locations, based on a combination of normalized average surge hydrographs derived from independent extremes of surge time series, average tide signal, and a scaling parameter adopted from the global COAST-RP dataset. These hydrographs are an improvement to the representation of the duration and shape of events resulting from ESLs and can replace the synthetic hydrographs in this study and past research.

Better representation and implementation of the flood protection levels is also a potential improvement that can be explored. Interpolated values for the protection levels could be replaced with more verified data subject to availability and the implementation of the protection structures within the SFINCS model via weirs could be developed further. A more automated and efficient process of creating the weirs' input is a potential area to be further looked into. More up to date and larger data sets of protection levels would lead to higher accuracy in the flood estimates and a better setup of weirs or thin dams along the coastlines.

For future research, the full extent of the European continent can be covered with the methodology and the supplementary material presented in this study. The input files can be easily generated and with the use of an HPC, the simulations can be carried out with consideration to the available resources and time. Also, other return periods or scenarios involving climate change could be researched further by applying the SFINCS solver. Any relevant SLR projections for such studies are to be based on IPCC Representative Concentration Pathways (RCPs) 4.5 and 8.5. Considering the current status of climate change policy implementation and carbon emissions, RCP 2.6 can be deemed to be improbable (University of Pittsburgh, 2022). With dynamic inundation modelling being a more appealing option, more accurate flood estimates for various different scenarios could be obtained and evaluated for future risk assessments and coastal flood adaptation measures.

Another recommendation that could be implemented in future research is to decrease the uncertainty caused by surface water and permanent water bodies during the post-processing of the flood outputs. Updated global datasets with the most recently formed water bodies could be adopted to increase the accuracy of the final results derived from the flood model outputs. With the above-mentioned recommendations, a comprehensive investigation of SFINCS outputs being compared to other dynamic modelling technique results could be conducted in the future.

Chapter 5 Conclusion

During this study, reduced-physics solver SFINCS was utilized to obtain coastal flood hazard estimates for European regions as computationally efficient dynamic inundation modelling techniques have been identified as a key tool in progressing towards improving flood risk assessments for research and decision-making on flood management. The main objective of this study was to develop a methodology to model and estimate coastal flooding extents on a continental scale using SFINCS, which has been proposed within this research. The applicability of SFINCS solver was successfully expanded to a larger scale, utilizing the input generation methods via MATLAB and QGIS.

Steps detailing how to generate the necessary inputs for the model setup, including the grid extents, elevation data, spatially varying friction data, boundary conditions, and protection structures are presented to answer part of the main research question that was formulated. The computational demand and efficiency were also evaluated, with the conclusion that an HPC such as the one used in this study is better suited to carry out a large-scale study using SFINCS for more accurate results in comparison to the traditional bathtub approach. A lower performance system cannot be deemed a viable option based on the simulation times obtained from this study. This could hinder the progress of obtaining outputs significantly.

Selected outputs obtained from SFINCS were compared against outputs from a GIS based inundation model applied on a global scale. Similarities and differences between the model results were identified but no significant general trend in the comparative analysis could be recognized. This could be associated with the variations in the modelling techniques, limitations within them, and potentially due to insufficient amount of data to make a comprehensive comparative analysis. Flood extent and depths obtained from the SFINCS models can be deemed satisfactory and do not appear to overestimate the flooding hazard with unrealistic results and an acceptable consensus with the compared output from previous research was obtained. To establish the accuracy of the SFINCS results, additional investigations are necessary which could be part of the scope for future studies.

Finally, as part of the research objectives and approach, limitations and potential improvements to the SFINCS model were discussed. Need for more detailed spatially varying friction values, low efficiency of slow processing computer systems with regards to the computational demand, simplistic synthetic hydrographs as forcing, limited flood protection data, and uncertainties in surface water data were identified as constraints of the study. As for developments, use of the SFINCS subgrid mode, storm tide hydrographs from recent literature instead of synthetic hydrographs, and improved implementation of flood protection measures were highlighted.

All in all, the methodology proposed in the study has the capability of applying SFINCS on the desired larger scale in an efficient manner and could be further applied and developed for obtaining coastal flood impact estimates in future studies focusing on Europe and beyond, subject to the availability of input data.

References

Ahn Y (2023) geotiff reader https://www.mathworks.com/matlabcentral/fileexchange/29425-geotiff-reader Access date 20-01-2023

Albano R, Sole A, Adamowski J, Perrone A, Inam A (2018) Using FloodRisk GIS freeware for uncertainty analysis of direct economic flood damages in Italy. International Journal of Applied Earth Observation and Geoinformation 73: 220-229 DOI 10.1016/j.jag.2018.06.019

Athif AA (2020) Computationally efficient modelling of wave driven flooding in Atoll Islands. Msc Thesis IHE Delft

Bates PD, Horritt MS, Fewtrell TJ (2010) A simple inertial formulation of the shallow water equations for efficient two-dimensional flood inundation modelling. Journal of Hydrology 387: 33-45 DOI 10.1016/j.jhydrol.2010.03.027

Bootsma J (2022) Evaluating methods to assess the coastal flood hazard on a global scale Msc Thesis University of Twente

Breilh JF, Chaumillon E, Bertin X, Gravelle M (2013) Assessment of static flood modeling techniques: application to contrasting marshes flooded during Xynthia (western France). Natural Hazards and Earth System Sciences 13: 1595-1612 DOI 10.5194/nhess-13-1595-2013

Chow VT (1959) Open Channel Hydraulics. McGraw-Hill, New York

Cialone MA, Amein M (1993) DYNLET1 Model Formulation and User's Guide COASTAL ENGINEERING RESEARCH CENTER VICKSBURG MS.

Copernicus (2020) CLC 2018 https://land.copernicus.eu/pan-european/corine-land-cover/clc2018?tab=download Access date 01-02-2023

Curtis KJ, Schneider A (2011) Understanding the demographic implications of climate change: estimates of localized population predictions under future scenarios of sea-level rise. Population and Environment 33: 28-54 DOI 10.1007/s11111-011-0136-2

Dangendorf S, Hay C, Calafat FM, Marcos M, Piecuch CG, Berk K, Jensen J (2019) Persistent acceleration in global sea-level rise since the 1960s. Nature Climate Change 9: 705-710 DOI 10.1038/s41558-019-0531-8

Dastgheib A (2022) Climate Change risk assessment in coastal areas and deltas IHE Delft

Dee DP, Uppala SM, Simmons AJ, Berrisford P, Poli P, Kobayashi S, Andrae U, Balmaseda MA, Balsamo G, Bauer P, Bechtold P, Beljaars ACM, van de Berg L, Bidlot J, Bormann N, Delsol C, Dragani R, Fuentes M, Geer AJ, Haimberger L, Healy SB, Hersbach H, Hólm EV, Isaksen L, Kållberg P, Köhler M, Matricardi M, McNally AP, Monge-Sanz BM, Morcrette JJ, Park BK, Peubey C, de Rosnay P, Tavolato C, Thépaut JN, Vitart F (2011) The ERA-Interim reanalysis: configuration and performance of the data assimilation system. Quarterly Journal of the Royal Meteorological Society 137: 553-597 DOI 10.1002/qj.828

Deltares (2022) SFINCS User Manual https://sfincs.readthedocs.io/en/latest/ Access date 10-10-2022

Dullaart JCM, Muis S, de Moel H, Ward PJ, Eilander D, Aerts JCJH (2022) DOI 10.5194/egusphere-2022-1048

Eilander D, Couasnon A, Leijnse T, Ikeuchi H, Yamazaki D, Muis S, Dullaart J, Winsemius HC, Ward PJ (2022) A globally-applicable framework for compund flood hazard modeling. EGUsphere 149 DOI 10.5194/egusphere-2022-149

Engwirda D (2023) INPOLY: A fast points-in-polygon test https://github.com/dengwirda/inpoly Access date 15-01-2022

EXCIMAP (2007) Handbook on good practices for flood mapping in Europe.

Goede Rd, Leijnse T, Ormondt Mv (2022) An introduction course into fast compound flood modelling - Learning to use the SFINCS model Deltares.
Gregory JM, Griffies SM, Hughes CW, Lowe JA, Church JA, Fukimori I, Gomez N, Kopp RE, Landerer F, Cozannet GL, Ponte RM, Stammer D, Tamisiea ME, van de Wal RSW (2019) Concepts and Terminology for Sea Level: Mean, Variability and Change, Both Local and Global. Surveys in Geophysics 40: 1251-1289 DOI 10.1007/s10712-019-09525-z
Hallegatte S, Green C, Nicholls RJ, Corfee-Morlot J (2013) Future flood losses in major coastal cities. Nature Climate Change 3: 802-806 DOI 10.1038/nclimate1979
Hinkel J, Feyen L, Hemer M, Le Cozannet G, Lincke D, Marcos M, Mentaschi L, Merkens JL, de Moel H, Muis S, Nicholls RJ, Vafeidis AT, van de Wal RSW, Vousdoukas MI, Wahl T, Ward PJ, Wolff C (2021) Uncertainty and Bias in Global to Regional Scale Assessments of Current and Future Coastal Flood Risk. Earth's Future 9 DOI 10.1029/2020ef001882
Hinkel J, Lincke D, Vafeidis AT, Perrette M, Nicholls RJ, Tol RS, Marzeion B, Fettweis X, Ionescu C, Levermann A (2014) Coastal flood damage and adaptation costs under 21st century sea-level rise. Proc Natl Acad Sci U S A 111: 3292-3297 DOI 10.1073/pnas.1222469111
Hinkel J, Nicholls RJ, Tol RSJ, Wang ZB, Hamilton JM, Boot G, Vafeidis AT, McFadden L, Ganopolski A, Klein RJT (2013) A global analysis of erosion of sandy beaches and sea-level rise: An application of DIVA. Global and Planetary Change 111: 150-158 DOI 10.1016/j.gloplacha.2013.09.002
Hinkel J, Nicholls RJ, Vafeidis AT, Tol RSJ, Avagianou T (2010) Assessing risk of and adaptation to sea-level rise in the European Union: an application of DIVA. Mitigation and Adaptation Strategies for Global Change 15: 703-719 DOI 10.1007/s11027-010-9237-y
IPCC (2014) Summary for policymakers. In: Climate Change 2014: Impacts, Adaptation, and Vulnerability. Part A: Global and Sectoral Aspects. Contribution of Working Group II to the Fifth Assessment Report of the Intergovernmental Panel on Climate Change.
Kirezci E, Young IR, Ranasinghe R, Muis S, Nicholls RJ, Lincke D, Hinkel J (2020) Projections of global-scale extreme sea levels and resulting episodic coastal flooding over the 21st Century. Sci Rep 10: 11629 DOI 10.1038/s41598-020-67736-6
Leijnse T, van Ormondt M, Nederhoff K, van Dongeren A (2021) Modeling compound flooding in coastal systems using a computationally efficient reduced-physics solver: Including fluvial, pluvial, tidal, wind- and wave-driven processes. Coastal Engineering 163 DOI 10.1016/j.coastaleng.2020.103796
Leijnse TWB (2018) Computationally Efficient Modelling of Compound Flooding due to Tropical Cyclones with the Explicit Inclusion of Wave-Driven Processes MSc thesis Delft University of Technology
Lesser GR, Roelvink JA, van Kester JATM, Stelling GS (2004) Development and validation of a three-dimensional morphological model. Coastal Engineering 51: 883-915 DOI 10.1016/j.coastaleng.2004.07.014
Lewis M, Bates P, Horsburgh K, Neal J, Schumann G (2013) A storm surge inundation model of the northern Bay of Bengal using publicly available data. Quarterly Journal of the Royal Meteorological Society 139: 358-369 DOI 10.1002/qj.2040
Marcos M, Rohmer J, Vousdoukas MI, Mentaschi L, Le Cozannet G, Amores A (2019) Increased Extreme Coastal Water Levels Due to the Combined Action of Storm Surges and Wind Waves. Geophysical Research Letters 46: 4356-4364 DOI 10.1029/2019gl082599

McGranahan G, Balk D, Anderson B (2016) The rising tide: assessing the risks of climate change and human settlements in low elevation coastal zones. Environment and Urbanization 19: 17-37 DOI 10.1177/0956247807076960
Muis S, Verlaan M, Winsemius HC, Aerts JC, Ward PJ (2016) A global reanalysis of storm surges and extreme sea levels. Nat Commun 7: 11969 DOI 10.1038/ncomms11969
Nicholls RJ, Hoozemans FMJ, Marchand M (1999) Increasing flood risk and wetland losses due to global sea-level rise: regional and global analyses. Global Environmental Change 9: S69-S87
Nicholls RJ, Lincke D, Hinkel J, Brown S, Vafeidis AT, Meyssignac B, Hanson SE, Merkens J-L, Fang J (2021) A global analysis of subsidence, relative sea-level change and coastal flood exposure. Nature Climate Change 11: 338-342 DOI 10.1038/s41558-021-00993-z
Nicholls RJ, Wong PP, Burkett VR, Codignotto JE, Hay RF, Ragoonaden S, Woodroffe CD (2007) Coastal systems and low-lying areasClimate Change 2007: Impacts, Adaptation and Vulnerability Contribution of Working Group II to the Fourth

Assessment Report of the Intergovernmental Panel on Climate Change:315-356.
Papaioannou G, Efstratiadis A, Vasiliades L, Loukas A, Papalexiou S, Koukouvinos A, Tsoukalas I, Kossieris P (2018) An Operational Method for Flood Directive Implementation in Ungauged Urban Areas. Hydrology 5 DOI 10.3390/hydrology5020024
Paprotny D, Morales-Nápoles O, Vousdoukas MI, Jonkman SN, Nikulin G (2018) Accuracy of pan-European coastal flood mapping. Journal of Flood Risk Management 12 DOI 10.1111/jfr3.12459
Parodi MU, Giardino A, van Dongeren A, Pearson SG, Bricker JD, Reniers AJHM (2020) Uncertainties in coastal flood risk assessments in small island developing states. Natural Hazards and Earth System Sciences 20: 2397-2414 DOI 10.5194/nhess-20-2397-2020
Pawlowicz R (2018) Read an ESRI-format shapefile https://github.com/g2e/m_map/blob/master/m_shaperead.m Access date 05-11-2022
Pekel JF, Cottam A, Gorelick N, Belward AS (2016) High-resolution mapping of global surface water and its long-term changes. Nature 540: 418-422 DOI 10.1038/nature20584
Peterse JGPMM (2016) Comparison of LISFLOOD-FP and Delft3D FM for large-scale flood inundation modelling Msc Thesis TU Delft
Porter J, Demeritt D (2012) Flood-Risk Management, Mapping, and Planning: The Institutional Politics of Decision Support in England. Environment and Planning A: Economy and Space 44: 2359-2378 DOI 10.1068/a44660
Ramirez JA, Lichter M, Coulthard TJ, Skinner C (2016) Hyper-resolution mapping of regional storm surge and tide flooding: comparison of static and dynamic models. Natural Hazards 82: 571-590 DOI 10.1007/s11069-016-2198-z
Ranasinghe R (2016) Assessing climate change impacts on open sandy coasts: A review. Earth-Science Reviews 160: 320-332 DOI 10.1016/j.earscirev.2016.07.011
Ranasinghe R (2022) HECEPD Module 8: Topic 2 - Hazards and risk assessment IHE Delft
Rey SJ (2015) Mathematical Models in Geography. International Encyclopedia of the Social & Behavioral Sciences (Second Edition): 785-790 DOI https://doi.org/10.1016/B978-0-08-097086-8.72033-2
Roelvink D, McCall R, Mehvar S, Nederhoff K, Dastgheib A (2018) Improving predictions of swash dynamics in XBeach: The role of groupiness and incident-band runup. Coastal Engineering 134: 103-123 DOI 10.1016/j.coastaleng.2017.07.004

Scussolini P, Aerts JCJH, Jongman B, Bouwer LM, Winsemius HC, de Moel H, Ward PJ (2016) FLOPROS: an evolving global database of flood protection standards. Natural Hazards and Earth System Sciences 16: 1049-1061 DOI 10.5194/nhess-16-1049-2016
Sebastian A, Bader DJ, Nederhoff CM, Leijnse TWB, Bricker JD, Aarninkhof SGJ (2021) Hindcast of pluvial, fluvial, and coastal flood damage in Houston, Texas during Hurricane Harvey (2017) using SFINCS. Natural Hazards 109: 2343-2362 DOI 10.1007/s11069-021-04922-3
Shen J (2023) geotiffwrite - Write a 2D or 3D array to a single or multi-band GeoTIFF file https://www.mathworks.com/matlabcentral/fileexchange/27959-geotiffwrite Access date 10-03-2023
Small C, Nicholls RJ (2003) A global analysis of human settlement in coastal zones. Journal of Coastal Research 19: 584-599
Stephen23 (2023) Natural-Order Filename Sort https://www.mathworks.com/matlabcentral/fileexchange/47434-natural-order-filename-sort Access date 08-11-2022
Stockdon HF, Holman RA, Howd PA, Sallenger AH (2006) Empirical parameterization of setup, swash, and runup. Coastal Engineering 53: 573-588 DOI 10.1016/j.coastaleng.2005.12.005
Tebaldi C, Ranasinghe R, Vousdoukas M, Rasmussen DJ, Vega-Westhoff B, Kirezci E, Kopp RE, Sriver R, Mentaschi L (2021) Extreme sea levels at different global warming levels. Nature Climate Change 11: 746-751 DOI 10.1038/s41558-021-01127-1
The European Space Agency (2021) Copernicus DEM - Global and European Digital Elevation Model (COP-DEM) https://spacedata.copernicus.eu/nl/collections/copernicus-digital-elevation-model Access date 31-03-2023
The H. John Heinz III Center for Science E, and the Environment (2000) The Hidden Costs of Coastal Hazards: Implications For Risk Assessment and Mitigation Island Press, Washington, DC
The Joint Research Centre (2015) European Extreme Storm Surge level - Historical http://data.europa.eu/89h/0026aa70-cc6d-4f6f-8c2f-554a2f9b17f2 Access date 03-02-2023
The World Bank (2010) World Development Report 2010: Development and Climate Change
The World Bank (2016) Methods in Flood Hazard and Risk Management International Bank for Reconstruction and Development/The World Bank
Tiggeloven T, de Moel H, Winsemius HC, Eilander D, Erkens G, Gebremedhin E, Diaz Loaiza A, Kuzma S, Luo T, Iceland C, Bouwman A, van Huijstee J, Ligtvoet W, Ward PJ (2020) Global-scale benefit–cost analysis of coastal flood adaptation to different flood risk drivers using structural measures. Natural Hazards and Earth System Sciences 20: 1025-1044 DOI 10.5194/nhess-20-1025-2020
UNDRR (n.d.) About UNDRR https://www.undrr.org/about-undrr Access date 01-03-2023
United States Army Corps of Engineers (1984) Shore Protection Manual 4th edition, 4 edn U.S. Army Corps of Engineers
United States Army Corps of Engineers (2002) CEM: Coastal Engineering Manual U.S. Army Corps of Engineers
University of Pittsburgh (2022) Future Climate Scenarios https://www.climatecenter.pitt.edu/climate-outreach/intergovernmental-panel-climate-change/future-climate-scenarios Access date 08-10-2022
Vafeidis AT, Schuerch M, Wolff C, Spencer T, Merkens JL, Hinkel J, Lincke D, Brown S, Nicholls RJ (2019) Water-level attenuation in global-scale assessments of exposure to

coastal flooding: a sensitivity analysis. Natural Hazards and Earth System Sciences 19: 973-984 DOI 10.5194/nhess-19-973-2019
Vitousek S, Barnard PL, Fletcher CH, Frazer N, Erikson L, Storlazzi CD (2017) Doubling of coastal flooding frequency within decades due to sea-level rise. Sci Rep 7: 1399 DOI 10.1038/s41598-017-01362-7
Vousdoukas MI, Bouziotas D, Giardino A, Bouwer LM, Mentaschi L, Voukouvalas E, Feyen L (2018c) Understanding epistemic uncertainty in large-scale coastal flood risk assessment for present and future climates. Natural Hazards and Earth System Sciences 18: 2127-2142 DOI 10.5194/nhess-18-2127-2018
Vousdoukas MI, Mentaschi L, Voukouvalas E, Bianchi A, Dottori F, Feyen L (2018b) Climatic and socioeconomic controls of future coastal flood risk in Europe. Nature Climate Change 8: 776-780 DOI 10.1038/s41558-018-0260-4
Vousdoukas MI, Mentaschi L, Voukouvalas E, Verlaan M, Jevrejeva S, Jackson LP, Feyen L (2018a) Global probabilistic projections of extreme sea levels show intensification of coastal flood hazard. Nat Commun 9: 2360 DOI 10.1038/s41467-018-04692-w
Vousdoukas MI, Voukouvalas E, Mentaschi L, Dottori F, Giardino A, Bouziotas D, Bianchi A, Salamon P, Feyen L (2016) Developments in large-scale coastal flood hazard mapping. Natural Hazards and Earth System Sciences 16: 1841-1853 DOI 10.5194/nhess-16-1841-2016
Warren I, Bach HK (1992) MIKE 21: a modelling system for estuaries, coastal waters and seas. Environmental Software 7: 229-240
Yamazaki D, Ikeshima D, Neal JC, O'Loughlin F, Sampson CC, Kanae S, Bates PD (2017) MERIT DEM: A new high-accuracy global digital elevation model and its merit to global hydrodynamic modeling, December 01, 2017
Yoshpe M (2023) Distance from points to polyline or polygon https://www.mathworks.com/matlabcentral/fileexchange/12744-distance-from-points-to-polyline-or-polygon Access date 01-11-2023
Zijlema M, Stelling G, Smit P (2011) SWASH: An operational public domain code for simulating wave fields and rapidly varied flows in coastal waters. Coastal Engineering 58: 992-1012 DOI 10.1016/j.coastaleng.2011.05.015

Appendices

Appendix A. - **Research Ethics Declaration Form**

Research Ethics Committee
IHE Delft Institute for
Water Education
E ResearchEthicsCommitee@un-ihe.org

Date: 2022-12-08
To: Hassaan Mohamed
MSc Programme: WSE-CEPD
Approval Number: IHE-RECO 2022-090

Subject: Research Ethics approval

Dear Hassaan Mohamed,

Based on your application for Ethical Approval, the Research Ethics Committee (RECO), IHE Delft RECO gives ethical clearance for your research topic Flood Impact Estimated for Europe due to Extreme Sea Levels

This approval valid until April 4, 2023. Please notify the RECO if your research protocol is modified in any way. If you do not complete your research by the specified date, contact RECO to request an extension for the ethical clearance.

Please keep this letter for your records and include a copy in the final version of your MSc. thesis, together with your personal ethics reflection.

On behalf of the Research Ethics Committee, I wish you success in the completion of your research.

Yours sincerely,

Dr. Angeles Mendoza Sammet
Coordinator, Research Ethics Committee IHE Delft

Copy to: Archive.

PO Box 3015, 2601 DA Delft, The Netherlands • Westvest 7, 2611 AX Delft • T +31 15 215 17 15 • info@un-ihe.org • www.un-ihe.org

Appendix B. - **Research Ethics Personal Statement**

As an independent and responsible researcher, for my MSc thesis, I have made every effort in my work to adhere to the ethical standards to the best of my ability. I have attempted to follow and keep my work in line with the key principles of Honesty, Transparency, Scrupulousness, Responsibility, and Independence.

I did my study with honesty and integrity, appropriately portraying my methodology plus results, and acknowledging sources that were utilized for information and ideas on the research topic. I have been transparent about my research methods and data collection processes, providing clear and detailed descriptions of how I developed the methodology and obtained the results. Any limitations of the study that were identified have been declared accordingly and improvements suggested to the best of my knowledge. The methodology for this research was developed in close association with the research mentor, with thorough discussions and consultations throughout the process. The process of obtaining the results was also discussed prior to carrying out the post-processing of the output data and the results presented have not been manipulated or altered to fit a particular outcome or agenda. Any steps taken to improve the results have been outlined for transparency.

Furthermore, during the research process, a meticulous approach was maintained in reviewing the literature, developing the methodology, and analysis of the outputs. Considering the time constraints, various details within the process were examined and a genuine attempt was made to not overlook any potential sources of bias or inaccuracies. Metrics used for statistical analysis were proven appropriate methods and the maps produced are presented with the necessary details and descriptions for completeness. I have considered the ethical implications of the research and arrived at appropriate conclusions based on the implemented methodology and analysis.

I acknowledge my responsibility to contribute positively to the broader coastal research community. The bulk of the work done for this study in terms of developing scripts and supplementary inputs for the models has been publicly shared for use. This can serve as a helpful resource for future studies in the field, enabling other researchers to replicate the study on a larger scale and improve upon it as highlighted in this study. In addition to being a responsible researcher, I have maintained my independence and have not allowed any sort of external pressures or prejudices to impact my results or conclusions. I conducted myself objectively and impartially, following the literature and results obtained. There is nothing to disclose in terms of conflicts of interest and no human or animal subjects were involved in the study.

Overall, I have done my best to uphold the ethical standards highlighted in Netherlands Code for Research Integrity and I am pleased to share this work with fellow researchers interested in coastal flooding and hazard assessments. I hope that this work will be beneficial to other researchers and that it will contribute to further improvements in the area. I believe that thorough and honest research is the best way to make scientific progress, and I am happy to have undertaken this study with those values in mind.

Appendix C. - **SFINCS Equations**

Equations driving the SFINCS model are presented below. These are adopted with reference to Leijnse (2018) and Athif (2020).

The mean option representing the water and bed levels in the x-direction is presented below:

$$h_{x,m,n+\frac{1}{2}}^{t-\Delta t} = \frac{\zeta_{m,n}^{t-\Delta t}+\zeta_{m,n+1}^{t-\Delta t}}{2} - \frac{d_{m,n}^{t-\Delta t}+d_{m,n+1}^{t-\Delta t}}{2} \quad \text{(E.1)}$$

Followed by the water depths, the momentum fluxes can be computed. This is done at the cell edges and the momentum equation in x-direction is as follows:

$$q_x^{t+\Delta t} = \frac{q_x^t - g.h_x^t.\frac{\Delta z}{\Delta x}.\Delta t}{(1+g.\Delta t.n^2.\frac{q_x^t}{h_x^{t\frac{7}{3}}})} \; where \; \frac{\Delta z}{\Delta x} = \frac{\zeta_{m+1,n}^{t-\Delta t}+\zeta_{m,n}^{t-\Delta t}}{\Delta x} \quad \text{(E.2)}$$

The discretization with the additional theta parameter is presented in E.3. This parameter is utilized to smoothen the flux state with implementation of a weighted average from the previous time step and the mean of fluxes from bordering cells in the same direction with a factor θ of default value 0.9.

$$q_{x,m+\frac{1}{2},n}^{t+\Delta t} = \frac{\left|\theta.q_{x,m+\frac{1}{2},n}^{t-\Delta t}+(1-\theta).\frac{q_{x,m+\frac{3}{2},n}^{t-\Delta t}+q_{x,m-\frac{1}{2},n}^{t-\Delta t}}{2}\right| - \Delta t(g.h_{x,m+\frac{1}{2},n}^{t-\Delta t}.\frac{\Delta z}{\Delta x})}{1+\Delta t.g.n^2.\frac{|q_{x,m+\frac{1}{2},n}^{t-\Delta t}|}{(h_{x,m+\frac{1}{2},n}^{t-\Delta t})^{\frac{7}{3}}}} \quad \text{(E.3)}$$

The momentum equation follows the same approach in the y-direction.

Advection and wind forcing terms are also included in the momentum equations. Input of the advection terms are controlled by the solver user.

$$q_x^{t+\Delta t} = \frac{q_x^t - \Delta t(g.h_x^t.\frac{\Delta z}{\Delta x}+adv_x-\frac{\tau_{w,x}}{\rho_w})}{1+\Delta t.g.n^2.\frac{q_x^t}{(h_x^t)^{\frac{7}{3}}}} \quad \text{(E.4)}$$

$$q_x^{t+\Delta t} = \frac{\theta.q_x^t - \Delta t(g.h_x^t.\frac{\Delta z}{\Delta x}+adv_x-\frac{\tau_{w,x}}{\rho_w})}{1+\Delta t.g.n^2.\frac{q_x^t}{(h_x^t)^{\frac{7}{3}}}} \quad \text{(E.5)}$$

Expression for the advection term is as follows:

$$adv_x = adv_{x,1D} + adv_{x,2D} \;\&\; adv_y = adv_{y,1D} + adv_{y,2D} \qquad \text{(E.6)}$$

The 1-D advection terms adopt the Upwind scheme and the 2-D term in included by employing the Central Difference scheme.

$$adv_{x,1D} = \frac{\left(\frac{\left(q^t_{x,m,n}\right)^2}{h^t_{x,m,n}} - \frac{\left(q^t_{x,m-1,n}\right)^2}{h^t_{x,m-1,n}}\right)}{\Delta x} \quad for\ q^t_{x,m,n} > 0 \qquad \text{(E.7)}$$

$$adv_{x,1D} = \frac{\left(\frac{\left(q^t_{x,m+1,n}\right)^2}{h^t_{x,m+1,n}} - \frac{\left(q^t_{x,m,n}\right)^2}{h^t_{x,m,n}}\right)}{\Delta x} \quad for\ q^{t-\Delta t}_{x,m,n} < 0 \qquad \text{(E.8)}$$

$$adv_{x,2D} = \frac{\frac{\frac{1}{2}\left(q^t_{x,m,n}+q^t_{x,m,n+1}\right)\cdot\frac{1}{2}\left(q^t_{x,m+1,n}+q^t_{x,m,n}\right)}{\frac{1}{2}\left(h^t_{x,m,n}+h^t_{x,m,n+1}\right)} - \frac{\frac{1}{2}\left(q^t_{x,m,n}+q^t_{x,m,n11}\right)\cdot\frac{1}{2}\left(q^t_{x,m+1,n-1}+q^t_{x,m,n-1}\right)}{\frac{1}{2}\left(h^t_{x,m,n}+h^t_{x,m,n-1}\right)}}{\Delta y} \qquad \text{(E.9)}$$

Similar expressions are applied for the $adv_{y,1D}$ and $adv_{y,2D}$.

After the calculation of the momentum fluxes, the continuity equation is utilized to update the water levels. This equation is discretized using an explicit and first order central difference approximation of the spatial momentum fluxes (BTCS-scheme).

$$\zeta^{t-\Delta t}_{m,n} = \zeta^t_{m,n} + \Delta t\left(\frac{\left(q^{t+\Delta t}_{x,m-1,n} - q^{t+\Delta t}_{x,m,n}\right)}{\Delta x} + \frac{\left(q^{t+\Delta t}_{y,m,n-1} - q^{t+\Delta t}_{y,m,n}\right)}{\Delta y} + S_{m,n}\right) \qquad \text{(E.10)}$$

Appendix D. - Information on the model setup scripts

All the MATLAB scripts and additional functions used in the methodology are available online and can be accessed with the link presented below:

- https://github.com/Hassaan-Mohamed/MSc-Thesis---Flood-Impact-Estimates-IHE-Delft-

The scripts developed during this study, which has been uploaded to the GITHUB repository is as follows:

- 1_GRID_GENERATION
  - Determining the orientation
  - Adjustment of grid points
  - Generating the grid information and main input files
  - Visualizing the grid extents
  - Creating the bounding box files

- 2_ELEVATION
  - Reprojection of the GeoTIFF files
  - Identifying applicable elevation data
  - Clipping the elevation data
  - Creating the sfincs.dep files
  - Creating the XYZ files

- 3_MASK
  - Defining the active, non-active, outflow boundary and water-level input boundary grid cells

- 4_FRICTION
  - Assigning the Manning roughness coefficients to the grid cells

- 5_BOUNDARY_CONDITIONS
  - Extracting data from the European Storm Surge Levels dataset
  - Creating the synthetic hydrographs
  - Creating the SFINCS forcing input files

- 6_PROTECTION_STRUCTURES
  - Setting up protection levels
  - Generating the missing data for the protection levels
  - Setting up the protection levels using the ESL data
  - Creating the sfincs.weir input files
  - Creating the sfincs.thd input files

- 7_BIN_INPUTS
  - Creating sfincs.dep, sfincs.man, sfincs.msk & sfincs.ind files

- 8_RESULTS_PROCESSING
  - Creating GeoTIFF files from the NetCDF format output files